TUDelft

Delft University of Technology

Document Version
Final published version

Contents lists available at ScienceDirect

Transportation Research Part C

journal homepage: www.elsevier.com/locate/trc

Distributionally robust optimization of sailing speed, bunkering, and fuel switching for dual-fuel liner services

Ping He [a,b], Lingxiao Wu [b,c,*], Jian Gang Jin [a], Shaorui Zhou [d,*],
Frederik Schulte [e]

[a] *School of Ocean and Civil Engineering, MOE Key Laboratory of Marine Intelligent Equipment and System, and State Key Laboratory of Ocean Engineering, Shanghai Jiao Tong University, Shanghai, China*
[b] *Department of Aeronautical and Aviation Engineering, The Hong Kong Polytechnic University, Hung Hom, Hong Kong*
[c] *The Hong Kong Polytechnic University Shenzhen Research Institute, Shenzhen 518057, China*
[d] *School of Intelligent Systems Engineering, Sun Yat-sen University, Guangzhou, China*
[e] *Faculty of Mechanical Engineering, Delft University of Technology, Delft, The Netherlands*

A B S T R A C T

To reduce CO_2 and SO_2 emissions, shipping companies have started deploying LNG or methanol dual-fuel ships on liner services. Unlike traditional container ships, these dual-fuel ships can use multiple types of fuels during a voyage, allowing them to comply with emission regulations while reducing operational costs through fuel switching and speed optimization. Given the significant fluctuations in bunker prices across different ports, decisions regarding fuel switching, refueling, and sailing speeds must account for price uncertainty. We develop a distributionally robust chance-constrained programming model based on the Wasserstein uncertainty set to minimize operating costs under this uncertainty. We divide each port-to-port sailing leg into sub-legs, considering regional emission requirements or canal segments. This segmentation enables the optimization of fuel usage proportions, sailing speeds, and refueling strategies for each sub-leg. The model is then reformulated as a tractable mixed-integer second-order conic programming model. We validate the model using real-world data from COSCO Shipping. Numerical experiments demonstrate that the model can identify optimal solutions for real-scale instances within practical computational time. Furthermore, the robust solutions significantly outperform those obtained using the traditional sample average approximation method. Our results suggest that the joint optimization of fuel management and sailing speeds for dual-fuel ships can effectively reduce operating costs without increasing emissions.

1. Introduction

Shipping transports more than 80% of global trade (UNCTAD, 2019; Wu et al., 2021) and thus plays a pivotal role in international trade and the global flow of goods. However, the shipping industry also contributes significantly to environmental pollution, as traditional marine fuels, such as Heavy Fuel Oil (HFO) and Marine Gas Oil (MGO), emit substantial amounts of sulfur or carbon emissions. Consequently, the International Maritime Organization (IMO) and other organizations, like the European Union, have introduced measures to promote the green transformation of the shipping industry. For instance, the IMO has established Emission Control Areas (ECAs), stipulating that the maximum sulfur content of fuel used in ECAs is 0.1% m/m (IMO). Additionally, since January 1,
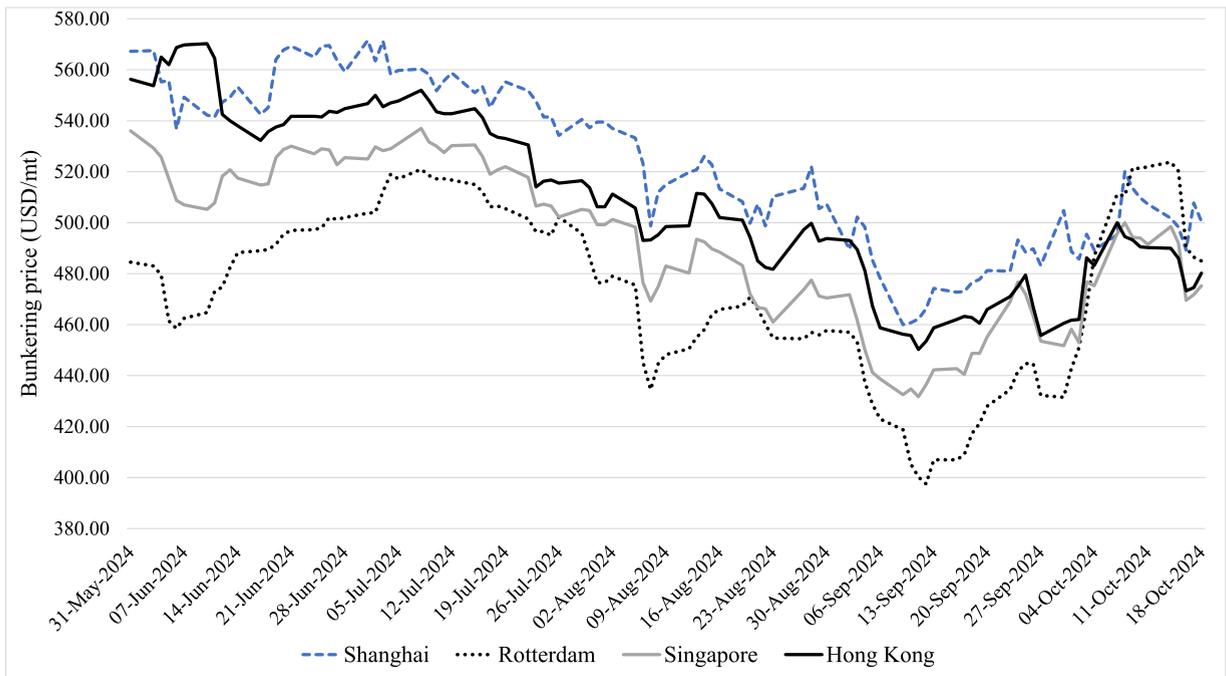
Fig. 1. HFO fuel prices at four ports over 100 days.

2023, the IMO's Carbon Intensity Indicator (CII) rating policy has been enforced to further regulate carbon and sulfur emissions from ship operations. These regulations are compelling shipping companies to transition to alternative fuels, such as Liquefied Natural Gas (LNG), methanol, and biofuel (Balcombe et al., 2019; Li et al., 2025), which offer lower sulfur and carbon emissions, to meet regulatory and climate requirements.

Despite the environmental benefits, the costs of using alternative fuels are significantly higher than those of traditional fuels. Consequently, the operating costs of ships using alternative fuels are notably increased, as fuel costs account for more than 60% of total operating expenses (Golias et al., 2009; Ronen, 2011; Wang et al., 2019). To mitigate the bunker costs of alternative-fueled ships, shipping companies have three primary strategies. First, they may adopt slow-steaming, which reduces sailing speeds to lower fuel consumption and emissions (Balcombe et al., 2019). However, excessively slow speeds may cause delays at port calls, potentially incurring penalties or compensation payments to shippers. Second, they can refuel at ports with lower fuel prices whenever possible. Nevertheless, fuel prices fluctuate significantly across ports and over time, as illustrated in Fig. 1. Third, they can implement a fuel-switching strategy by adopting LNG or methanol dual-fuel ships. Capable of utilizing both conventional and alternative fuels, these vessels represent a core emerging technology in the shipping industry's strategic decarbonization roadmap.

Even in studies that consider fuel switching, the scope has been limited to traditional vessels, focusing on the mandatory switch: adopting MGO or other conventional low-sulfur fuels before entering an ECA and reverting to HFO outside. Dual-fuel ships are typically equipped with separate tanks for traditional fuels (such as HFO and MGO) and alternative fuels (such as LNG and methanol), enabling operators to switch fuels between multiple types during voyages to minimize costs (Wu et al., 2024; Shangguan et al., 2025). However, this operational flexibility introduces significant new trade-offs and constraints not seen in traditional shipping. Alternative fuels are not yet widely deployed, and ports with alternative fueling capabilities are limited (Li et al., 2025). Consequently, the use of these fuels requires special consideration of supply capacity to prevent fuel shortages during voyages. Furthermore, operators must navigate a new, complex trade-off between fuel costs and carbon emission costs. Using one tonne of LNG, HFO, and MGO emits 2.75, 3.14, and 3.25 tonnes of carbon dioxide, respectively. While LNG is the preferred option for reducing carbon emissions, it is generally more expensive, and exclusive reliance on it can lead to significantly higher operating costs. These factors significantly complicate the liner service operation of dual-fuel ships (Tan et al., 2020). For instance, for a single voyage leg (whether inside or outside an ECA), operators must decide on the proportion of sail powered by alternative fuels versus traditional fuels, along with the corresponding sailing speed, to minimize the total operating cost while satisfying fuel supply constraints. As such, the introduction of dual-fuel ships, while offering significant environmental advantages, also introduces novel and intricate operational challenges that traditional shipping models do not adequately address.

However, current studies typically focus on liner services of traditional ships (Wang and Meng, 2015; Aydin et al., 2017; Zhen et al., 2017; Liu et al., 2019), and thus fail to capture the unique operational complexities introduced by emerging dual-fuel ship technologies. More fundamentally, while prior research has examined the tactical decision of route evasion to avoid ECAs, these findings are generally not applicable to the fixed, scheduled nature of liner services. Furthermore, current studies assume that fuel prices are deterministic or follow a predefined distribution. As shown in Fig. 1 and highlighted by Wang et al. (2018), fuel prices

fluctuate irregularly over time and do not follow a common distribution function. These make the proposed models unsuitable for the operation of dual-fuel liner services. To fill these gaps and address the novel operational challenges posed by dual-fuel ships operating in an uncertain environment, this study investigates the joint optimization of sailing speed, fuel switching, and refueling strategies for liner services of dual-fuel ships. The primary objective is to minimize operating costs for a round-trip service while accounting for bunker price uncertainty. Given the difficulty in accurately determining the distribution of fluctuating bunker prices and the need to avoid the excessive conservatism of traditional robust optimization approaches, we employ the Distributionally Robust Optimization (DRO) framework, which strategically balances solution robustness with economic efficiency. We construct a distributionally robust chance constraint model using historical bunker prices with the Wasserstein ball uncertainty set. Next, we reformulate this model into a mixed-integer second-order conic programming (MISOCP) model, which can be exactly solved using off-the-shelf solvers such as CPLEX. Our work makes the following main contributions:

(1) We examine the operational challenges of integrating LNG dual-fuel ships, a pivotal, high-cost, but emerging technology for maritime decarbonization, into liner services. Then, we propose a novel optimization problem that integrates sailing speed, fuel switching, and refueling strategies for dual-fuel ships in liner services.

(2) We build a new mixed-integer linear programming (MILP) model with the objective of minimizing the total cost of liner services for the problem under deterministic fuel prices. The model incorporates multiple constraints, including those related to emission, fuel refueling and switching, fuel usage and sailing speed, and liner service schedule.

(3) We propose a chance-constraint model considering bunker price uncertainty. Then, we utilize the Wasserstein uncertainty set to portray the distribution ambiguity of bunker prices and formulate a distributionally robust chance-constrained programming model. This novel model is equivalently converted into a tractable MISOCP formulation.

(4) Using real-world data from COSCO Shipping, we provide the first evidence that the proposed approach offers tangible economic advantages for dual-fuel liner shipping. Our computational results demonstrate the models' effectiveness in cost minimization and demonstrate the robustness of the proposed approach under bunker price uncertainty.

The remainder of this study is organized as follows: Section 2 reviews the related literature and identifies the research gaps. Section 3 elaborates on the investigated problem and presents the deterministic, chance-constrained, and distributionally robust chance-constrained models. Numerical experiments and management insights are presented in Section 4. Finally, the conclusions are summarized in Section 5.

2. Literature review

This study is closely related to three key streams of research: (1) optimization of sailing speeds and bunkering strategies, (2) optimization of liner services under uncertain fuel prices, and (3) optimization of liner services under emission control policies.

2.1. Optimization of sailing speeds and bunkering strategies

Sailing speed and bunkering strategy optimization is a classical problem in shipping operations that has been extensively studied. Many researchers have focused on reducing operating costs through optimizing sailing speeds or bunkering strategies. For instance, Fagerholt et al. (2010) developed a nonlinear programming model to optimize sailing speeds of a tramp shipping route, approximating fuel consumption as a cubic function of speeds. Norstad et al. (2011) introduced a tramp ship routing and scheduling problem with sailing speed optimization and proposed a heuristic algorithm to solve it. Psaraftis and Kontovas (2014) developed models to optimize sailing speeds of a single ship, integrating factors such as fuel prices, freight rates, and inventory costs. With the implementation of strict sulfur emission limits in ECAs, Fagerholt et al. (2015) developed a mixed-integer programming model to jointly optimize sailing paths and speeds while considering ECAs. Meng et al. (2015) introduced the tramp ship routing and bunkering problem, which jointly optimized the bunkering strategy and routing decisions under fixed sailing speeds. Zhen et al. (2017) investigated an optimal bunkering policy for liner shipping and proposed a dynamic programming algorithm to derive the best control strategy. Omholt-Jensen et al. (2025) investigated the tramp ship routing and scheduling problem with bunker optimization, aiming to maximize total profit. To solve this problem, they proposed a math-heuristic algorithm based on a path flow model.

Simultaneously, several studies have attempted to jointly optimize fuel management and sailing speeds. Wang and Meng (2015) investigated a joint optimization problem of sailing speeds and refueling strategy in liner shipping, and developed a mixed-integer nonlinear programming formulation to minimize total costs. Aydin et al. (2017) employed dynamic programming to optimize sailing speed and bunkering in liner shipping while accounting for service times and time window uncertainties. Liu et al. (2019) investigated a liner ship bunkering and speed optimization problem with transport demand uncertainty, proposing a two-stage stochastic nonlinear model solved through the Sample Average Approximation (SAA) approach. More recently, He et al. (2024) investigated the joint optimization of routing, sailing speeds, and bunkering decisions for LNG-fueled tramp ships, considering alternative bunkering ports. These studies demonstrate that jointly optimizing bunkering strategies and sailing speeds can effectively reduce emissions and operational costs without impeding shipping performance.

2.2. Optimization of liner service under uncertain fuel prices

The problem of optimizing liner services under fuel price uncertainty has garnered increasing attention in recent years. Sheng et al. (2015) addressed the bunkering and speed optimization problem by implementing a dynamic inventory policy that accounts for uncertainties in bunker prices and fuel consumption. Similarly, Zhen et al. (2017) incorporated stochastic fuel consumption and

bunker prices into their model for liner shipping, proposing a dynamic programming algorithm to derive the optimal bunkering policy. Lashgari et al. (2021) developed a scenario-based stochastic mixed-integer linear programming formulation to optimize the sailing speed, bunkering policy, and ship route under uncertain bunker prices.

However, these studies rely on the assumption that fuel price uncertainty can be represented by a predefined distribution. For instance, Sheng et al. (2015) and Lashgari et al. (2021) employed multiple discrete scenarios to model fuel price uncertainty. As Wang et al. (2018) pointed out, fuel prices are usually not characterized by a well-defined distribution, making such assumptions less reliable. To address this limitation, Wang et al. (2018) proposed a distribution-free mixed-integer second-order conic programming model to approximate the optimal sailing speeds and bunkering quantities for a linear shipping line. The model utilized the lower and upper bounds, means, and covariances of historical bunker prices to estimate the uncertainty.

2.3. Optimization of liner service under emission control policies

The evolution of maritime emission control policies has profoundly reshaped the complexity of liner shipping operations management (Zhen et al., 2024). Early research on shipping emission control predominantly focused on the ECA policy, which mandates the use of low-sulfur fuel, such as MGO, within designated zones (Fagerholt and Psaraftis, 2015). In response, a few studies have been dedicated to optimizing shipping services under ECA regulations (Zhen et al., 2020; Zhuge et al., 2021; Wang et al., 2021; Zhen et al., 2024). Fagerholt et al. (2015) investigated the joint optimization of vessel routes and speeds, suggesting that ships adopt different speeds inside and outside ECAs and may even reroute to reduce the consumption of expensive low-sulfur fuel. However, such rerouting strategies, while shortening the distance sailed within ECAs, can lead to an increase in total emissions due to a longer overall voyage. Building on this, Zhou and Wang (2025) further explored the joint optimization of vessel speed and routing under fuel price uncertainty. However, all of these studies were based on the traditional fuel-switching model for ships, where low-sulfur fuel is used within ECAs and conventional HFO is used outside. The core of these fuel-related decisions revolved around optimizing bunkering strategies (location and volume). Consequently, the complexity of operational management was primarily manifested in route and speed adjustments (Gao et al., 2025).

In recent years, the shipping industry's decarbonization challenge has escalated from complying with a single sulfur limit to navigating dual constraints on both sulfur and carbon emissions (Zhuge et al., 2024). This paradigm shift has been driven by the full implementation of the IMO 2020 global sulfur cap, complemented by the introduction of mandatory carbon reduction measures such as the Carbon Intensity Indicator (CII) and the European Union Emissions Trading System (EU-ETS) (Wang et al., 2025a,b). In response, LNG or methanol dual-fuel vessels capable of using alternative fuels such as LNG, methanol, and ammonia have seen large-scale adoption, which, in turn, has created new operational management problems (Wu et al., 2024; Shangguan et al., 2025). Although these dual-fuel ships offer an effective solution for emission reduction, the number of ports with alternative fuel supply capabilities remains limited (Li et al., 2023; He et al., 2024; Li et al., 2025). Furthermore, the fuel-switching decision-making has evolved from a simple "either-or" choice between conventional fuels to a "multi-fuel portfolio" approach. Modern dual-fuel vessels can carry both conventional and alternative fuels, necessitating fuel-switching decisions to determine the optimal mix and usage ratio of different fuels for each voyage leg (both inside and outside ECAs) (Shangguan et al., 2025). These fuel-use decisions, compounded by significant differences in emission factors and bunkering prices among various fuels, have rendered vessel operational decisions unprecedentedly complex.

2.4. Research gaps

While previous studies primarily focus on tactical route design or operational speed and bunkering optimization for conventional vessels, our research contributes to the literature by addressing several critical gaps. First, few studies address the integrated operational problem specific to LNG dual-fuel liner services. This novel operational problem requires the joint determination of the optimal fuel mix and usage ratio, bunkering volume, and vessel speeds for every voyage leg. This significantly differentiates our work from prior studies, such as Fagerholt et al. (2015), which primarily focused on route redesign considering the impact of using different fuels within and outside the ECAs (MGO in ECAs, HFO outside). Second, existing studies on operational sailing speed and refueling optimization have given limited attention to fuel price uncertainty, and rely on restrictive assumptions that fail to accurately capture the distribution-free nature of this uncertainty.

To fill these critical gaps, we propose a joint optimization framework that integrates sailing speed, fuel switching, and refueling strategies for LNG dual-fuel liner services. To account for the distributional ambiguity of fuel prices, we employ the Wasserstein uncertainty set to portray it. Based on this, we develop a distributionally robust chance-constrained programming model and reformulate it into an equivalent and computationally tractable mixed-integer second-order conic programming model.

3. Robust optimization of sailing speed, fuel switching, and refueling strategies for liner services with dual-fuel ship

Consider an LNG dual-fuel container ship assigned to a round-trip transportation service for a liner shipping line. The ship must sequentially call at a predefined set of ports $\mathcal{P}$. Each port of call is restricted to an earliest time of berthing e_i and a latest time of berthing l_i. Specifically, if the ship arrives before the earliest time e_i, it must wait at the anchorage until e_i. Conversely, if the ship arrives after l_i, there will be a delay cost. After berthing at the port, the ship begins bunkering, loading, and unloading operations.

Let $\mathcal{L}_{ij}$ denote the voyage leg between two consecutive ports i and j. Due to geographical locations and environmental regulations, this leg may be partitioned into a set of sub-legs, S_{ij}. A sub-leg $s \in S_{ij}$ is defined as a section of leg $\mathcal{L}_{ij}$ where the emission regulation
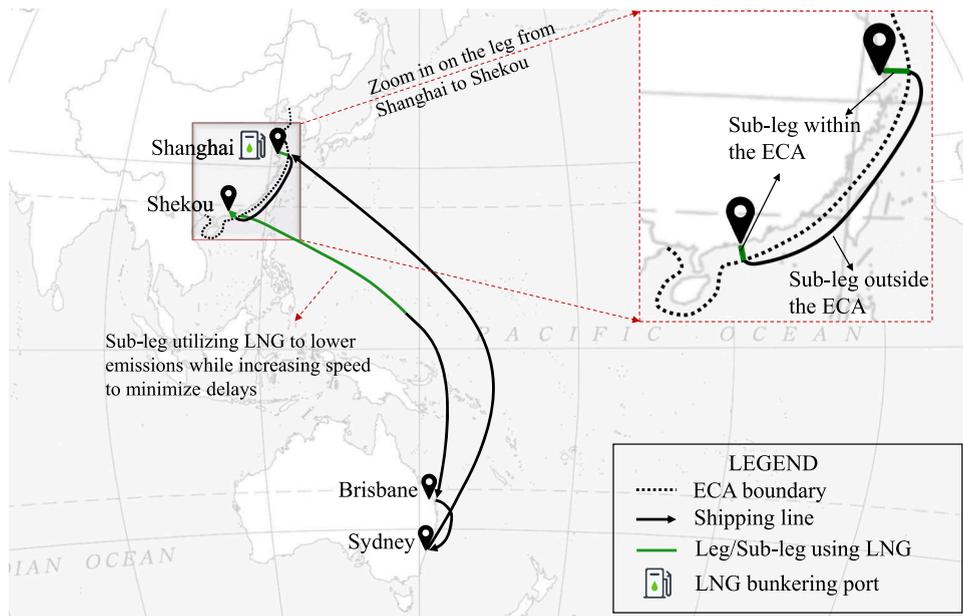
Fig. 2. Illustrative example of a liner shipping line with LNG dual-fuel ship.

status (inside or outside an ECA) is uniform throughout its entirety. The division into sub-legs is precisely determined by the physical crossing of ECA boundaries (Shangguan et al., 2025). This partitioning is essential because the allowed set of fuels (high-sulfur vs. low-sulfur) changes at these geographical points. Fig. 2 illustrates an example of a shipping line with four legs for an LNG dual-fuel container ship. The ship departs from Shanghai and sequentially calls at Shekou, Brisbane, and Sydney before returning to Shanghai. The leg from Shanghai to Shekou crosses an ECA twice. Consequently, this leg is partitioned into three distinct sub-legs: two within the ECA and one outside. For the sub-legs within the ECA, the ship may use LNG or MGO, whereas for the sub-leg outside, it can utilize HFO, MGO, or LNG.

Unlike traditional ships, the LNG dual-fuel vessel can use both conventional fuels (HFO and MGO) and alternative fuel (LNG) during its voyages. The operational fuel switching of a dual-fuel ship differs significantly from the mandatory, regulatory-driven switching (such as HFO to MGO/VLSFO) performed by conventional ships solely for ECA compliance. Dual-fuel ships possess greater flexibility, enabling operators to switch fuels between multiple types (HFO, MGO, and LNG) on any sub-leg to actively minimize costs. Due to the high sulfur emissions, HFO cannot be used in ECA regions, making LNG or MGO mandatory in these areas. Furthermore, using one tonne of LNG, HFO, and MGO emits 2.75, 3.14, and 3.25 tonnes of carbon dioxide, respectively, making LNG the preferred option for reducing carbon emissions.

While LNG is the preferred option for reducing emissions, it is generally more expensive, and exclusive reliance on it can lead to significantly higher operating costs. More importantly, LNG refueling is often only available at hub ports (as highlighted in Fig. 2), which severely limits bunkering options and necessitates careful forward planning. Therefore, the operational complexity is compounded by the need to strike an optimal balance between fuel costs (subject to highly fluctuated fuel prices), limited refueling capacity, and emission expenses. Designing optimal liner services under these conditions requires a joint optimization approach. This ultimately involves determining the optimal types and proportions of fuels to use (associated with an optimal sailing speed) on each sub-leg, as well as optimal bunkering decisions at ports, all aimed at minimizing overall operating costs.

To facilitate the modeling, we make the following assumptions: (1) the effects of wind, waves, and currents on fuel consumption are not considered; (2) auxiliary engines use the same type of fuel as the main engine during the sailing and switch to LNG fuel after berthing in ports; (3) mooring, loading, and unloading times are fixed, without considering variations caused by factors such as port congestion; and (4) fuel bunkering can occur simultaneously with the loading and unloading of the ship, and its duration is typically shorter than the loading and unloading time at ports. Therefore, the time required for refueling is not accounted for separately. To ensure the safety of operations, the setting up and disconnecting of the filling pumps before and after the fuel refueling cannot be conducted concurrently with the loading and unloading of the cargo. Therefore, there will be a fixed setup time for each refueling task.

All parameters and variables necessary for model development are listed in Tables 1, 2, and 3.

3.1. Deterministic model

Building on the above description and parameter definitions, a deterministic mathematical model is developed to optimize sailing speeds, fuel switching, and refueling strategies for liner services, as presented below:

Table 1
Sets for the mathematical model.

Notations	Descriptions
$\mathcal{P}$	Set of ports along the shipping line
$\mathcal{L}$	Set of legs between any two adjacent ports along the shipping line
S_{ij}	Set of sub-legs of the leg from port i to port j, where $i,j \in \mathcal{P}$ and leg $(i,j) \in \mathcal{L}$
S_{ij}^{ECA}	Set of sub-legs within the ECA area of leg $(i,j) \in \mathcal{L}$
$\mathcal{V}$	Set of alternative speeds
$\mathcal{V}_s$	Set of alternative speeds which can be used in sub-leg $s \in S_{ij}$
$\mathcal{F}$	Set of fuel types that the ship can use
$\mathcal{F}^H$	Set of fuels with high sulfur
$\mathcal{F}_i$	Set of fuels can be refueled at port $i \in \mathcal{P}$

Table 2
Parameters for the mathematical model.

Notations	Descriptions
Δ_{vf}	Fuel consumption rate (mt/h) of the main engine when the ship sails at speed v using fuel $f \in \mathcal{F}$
δ_f	Fuel consumption rate (mt/h) of auxiliary engines when using fuel $f \in \mathcal{F}$
p_f^i	Average bunker price of fuel $f \in \mathcal{F}$ at port $i \in \mathcal{P}$
ϕ_f	Carbon emission factor of fuel $f \in \mathcal{F}$
t_{sv}^{ij}	Sailing time (hours) required for the ship to pass through sub-leg $s \in S_{ij}$ of leg $(i,j) \in \mathcal{L}$ at speed $v \in \mathcal{V}_s$
q_f^{ub}	Fuel tank capacity (mt) for fuel $f \in \mathcal{F}$
q_f^{lb}	Minimum residual fuel volume (mt) required upon arrival at a port when using fuel $f \in \mathcal{F}$
τ_i	Loading and unloading time (hours) at port $i \in \mathcal{P}$
γ_i	Penalty cost (USD per hour) incurred if the ship arrives later than the latest time of berthing at port $i \in \mathcal{P}$
e_i	Earliest start time of berthing at port $i \in \mathcal{P}$
l_i	Latest start time of berthing at port $i \in \mathcal{P}$
λ	Set up time for refueling
η	Emission cost per ton of CO_2 emitted

Table 3
Decision variables for the mathematical model.

Notations	Descriptions
$x_{svf}^{ij} \in [0,1]$	Proportion of nautical miles traveled using fuel $f \in \mathcal{F}$ at speed $v \in \mathcal{V}_s$ in sub-leg $s \in S_{ij}$
$\zeta_f^i \in \{0,1\}$	Whether the ship bunkers fuel $f \in \mathcal{F}$ at port $i \in \mathcal{P}$
$a_i \geq 0$	Arrival time at port $i \in \mathcal{P}$
$d_i \geq 0$	Departure time from port $i \in \mathcal{P}$
$\psi_i \geq 0$	Arrival delay time at port $i \in \mathcal{P}$
$b_f^i \geq 0$	Amount of fuel $f \in \mathcal{F}$ refueled at port $i \in \mathcal{P}$
$q_f^i \geq 0$	Amount of remaining fuel $f \in \mathcal{F}$ when the ship arrives at port $i \in \mathcal{P}$

$$[MILP] \min \sum_{i \in \mathcal{P}} \sum_{f \in \mathcal{F}} p_f^i b_f^i + \sum_{i \in \mathcal{P}} \gamma_i \psi_i + \sum_{(i,j) \in \mathcal{L}} \sum_{s \in S_{ij}} \sum_{v \in \mathcal{V}_s} \sum_{f \in \mathcal{F}} \eta \phi_f (\Delta_{vf} + \delta_f) t_{sv}^{ij} x_{svf}^{ij} + \sum_{i \in \mathcal{P}} \eta \phi_{LNG} \delta_{LNG} \tau_i \tag{1}$$

$$s.t. \sum_{v \in \mathcal{V}_s} \sum_{f \in \mathcal{F}} x_{svf}^{ij} = 1, \forall (i,j) \in \mathcal{L}, \forall s \in S_{ij}, \tag{2}$$

$$\sum_{v \in \mathcal{V}_s} x_{svf}^{ij} = 0, \ \forall (i,j) \in \mathcal{L}, s \in S_{ij}^{ECA}, f \in \mathcal{F}^H, \tag{3}$$

$$q_f^i \geq q_f^{lb}, \ \forall i \in \mathcal{P}, \forall f \in \mathcal{F}, \tag{4}$$

$$b_f^i = 0, \quad \forall i \in \mathcal{P}, \forall f \in \mathcal{F} \backslash \mathcal{F}_i, \tag{5}$$

$$q_f^i + b_f^i \leq q_f^{ub}, \ \forall i \in \mathcal{P}, \forall f \in \mathcal{F}, \tag{6}$$

$$q_f^j = q_f^i + b_f^i - \sum_{s \in S_{ij}} \sum_{v \in \mathcal{V}_s} \left(\Delta_{vf} + \delta_f \right) t_{sv}^{ij} x_{svf}^{ij} - \delta_f \tau_i, \ \forall (i,j) \in \mathcal{L}, \forall f \in \{LNG\}, \tag{7}$$

$$q_f^j = q_f^i + b_f^i - \sum_{s \in S_{ij}} \sum_{v \in V_s} (\Delta_{vf} + \delta_f) t_{sv}^{ij} x_{svf}^{ij}, \ \forall (i,j) \in \mathcal{L}, \forall f \in \mathcal{F} \backslash \{LNG\}, \tag{8}$$

$$M\zeta_f^i \geq b_f^i, \ \forall i \in \mathcal{P}, \forall f \in \mathcal{F}_i, \tag{9}$$

$$d_i \geq a_i + \tau_i + \lambda \sum_{f \in \mathcal{F}_i} \zeta_f^i, \ \forall i \in \mathcal{P}, \tag{10}$$

$$d_i \geq e_i + \tau_i + \lambda \sum_{f \in \mathcal{F}_i} \zeta_f^i, \ \forall i \in \mathcal{P}, \tag{11}$$

$$d_i + \sum_{s \in S_{ij}} \sum_{v \in V_s} \sum_{f \in \mathcal{F}} t_{sv}^{ij} x_{svf}^{ij} \leq a_j, \ \forall (i,j) \in \mathcal{L}, \tag{12}$$

$$\psi_i \geq a_i - l_i, \ \forall i \in \mathcal{P}, \tag{13}$$

$$x_{svf}^{ij} \in [0,1], \ \forall (i,j) \in \mathcal{L}, s \in S_{ij}, v \in \mathcal{V}, f \in \mathcal{F}, \tag{14}$$

$$\zeta_f^i \in \{0,1\}, \ \forall f \in \mathcal{F}, i \in \mathcal{P}, \tag{15}$$

$$b_f^i \geq 0, \ \forall i \in \mathcal{P}, f \in \mathcal{F}, \tag{16}$$

$$q_f^i \geq 0, \ \forall i \in \mathcal{P}, f \in \mathcal{F}, \tag{17}$$

$$a_i \geq 0, d_i \geq 0, \psi_i \geq 0, \ \forall i \in \mathcal{P}. \tag{18}$$

The objective function (1) minimizes total costs, including bunker costs, penalties for actual berthing times exceeding the corresponding latest times, and CO_2 emission costs for this liner service. Constraints (2) select the speed and fuel used for each sub-leg, allowing multiple speeds and fuels within a single sub-leg. Constraints (3) prohibit the use of high-sulfur fuels within ECAs. Constraints (4) ensure that the remaining amount of each fuel at each port is greater than a specified minimum threshold. Constraints (5) enforce that if port i does not supply fuel f, the corresponding bunkering amount for fuel f at this port is zero. Constraints (6) ensure that the sum of the remaining amount and the bunkering amount of fuel f at port i does not exceed the tank capacity of fuel f. Constraints (7) and (8) determine the remaining fuel amount after sailing from port i to port j. When a ship is berthed at a port, its auxiliary engines utilize LNG fuel. Consequently, the total LNG fuel consumption must account for both sailing and port times. This distinction underpins the need to separately define the remaining fuel amounts for LNG and other fuels in constraints (7) and (8), respectively. Constraints (9) indicate whether fuel f is bunkered at port i. Here, M represents a sufficiently large constant and can be set as q_f^{ub}. Constraints (10)-(12) specify the departure time from port i and the arrival time at port j, respectively. Constraints (13) calculate the delay at each port. Constraints (14)-(18) define the domain of decision variables.

3.2. Chance constraint model

The fluctuation of bunker prices tends to be significant over several months. For instance, the price of MGO fuel at the port of Singapore was \$782.0/mt on May 1, 2024, but it dropped to \$672.5/mt by November 1, 2024. In addition, a round-trip liner service typically spans several months. Therefore, uncertainties in fuel prices must be taken into account to minimize bunker costs. Otherwise, the fluctuation of fuel prices may lead to higher bunker costs associated with the solution of the deterministic model. To balance the economic efficiency and risk of the refueling strategy, we introduce a chance constraint to incorporate this uncertainty. Let Θ denote the expected bunker cost, and the chance constraint ensures that the probability of the expected bunker cost being greater than the actual bunker cost is no less than $1 - \varepsilon$, where ε represents the confidence level of the chance constraint. Let $\tilde{p}_f^i$ represent the random bunker price for fuel $f \in \mathcal{F}$ at port $i \in \mathcal{P}$. Then, the original MILP model can thus be reformulated as the following chance-constrained model:

$$[\text{CCP}] \min \Theta + \sum_{i \in \mathcal{P}} \gamma_i \psi_i + \sum_{(i,j) \in \mathcal{L}} \sum_{s \in S_{ij}} \sum_{v \in V_s} \sum_{f \in \mathcal{F}} \eta \phi_f (\Delta_{vf} + \delta_f) t_{sv}^{ij} x_{svf}^{ij} + \sum_{i \in \mathcal{P}} \eta \phi_{LNG} \delta_{LNG} \tau_i \tag{19}$$

$$s.t.\ \mathbb{P}\Big[\Theta \geq \sum_{i\in\mathcal{P}}\sum_{f\in\mathcal{F}}\tilde{p}_f^i b_f^i\Big] \geq 1-\varepsilon, \tag{20}$$

$$(2)-(18), \text{and } \Theta \geq 0. \tag{21}$$

The objective function (19) aims to minimize the expected bunker costs, delay costs, and emission costs. Chance constraint (20) specifies that the probability that the actual bunker cost under random bunker prices is less than the expected bunker cost Θ is at least $1-\varepsilon$. Constraint (21) defines the decision variables.

Since the distribution of fuel bunker prices is typically unknown and does not exhibit common distributional characteristics, it is not feasible to solve the model using equivalent transformation methods. Therefore, we employ the SAA method to solve it. The details of employing the SAA method to solve the CCP model are presented in Appendix A.

3.3. Distributionally robust chance constraint model

As mentioned earlier, one of the core operational challenges in this study arises from the significant uncertainty in fuel prices since the exact distribution of fuel bunker prices is unknown and does not exhibit common distributional characteristics. To model this challenge, we employ the Distributionally Robust Optimization (DRO) framework, which combines the strengths of frequently used Stochastic Programming (SP) and Robust Optimization (RO) while mitigating their drawbacks. First, the DRO approach is data-driven and distribution-free, enabling it to learn the structure of uncertainty directly from limited historical samples, which effectively relaxes the restrictive distributional assumptions required by SP. Furthermore, DRO allows decision-makers to specify a set of potential probability distributions (the uncertainty set) for the uncertain parameters, rather than committing to a single, precise distribution as in SP. Second, unlike traditional Robust Optimization (RO), which is often overly conservative, DRO offers greater flexibility in managing uncertainty. This flexibility enables a better balance between robustness and performance, as decision-makers can control the level of conservatism through uncertainty sets, such as the Wasserstein radius (θ). Third, the Wasserstein distance ambiguity set not only accounts for potential outcomes of bunker prices not observed in historical data but also ensures a tractable reformulation of the robust liner service optimization problem.

In summary, the DRO approach provides a data-driven (learning from limited data), distribution-free (avoiding restrictive assumptions), and flexible (allowing decision-makers to control conservatism) approach. Therefore, the DRO approach is particularly suitable for modeling the chance constraint, leading to the formulation of our Distributionally Robust Chance Constraint (DRCC) model with a Wasserstein uncertainty set.

We assume that $\tilde{\mathbf{p}}$ represents random bunker prices, whose true distribution $\mathbb{Q}$ is not exactly known but can be partially observed via historical samples. Let $\mathbf{p}_n$ denote the n-th historical sample of these random prices, where $n \in \{1, 2, \dots N\}$, and N is the total number of independent samples. Based on these samples, we can construct a discrete empirical distribution $\hat{\mathbb{Q}}$, with its point mass function defined as $\hat{\mathbb{Q}}_N\{\tilde{\mathbf{p}}=\hat{\mathbf{p}}\} = 1/N$, where $\hat{\mathbf{p}}$ represents the empirical random variables.

The empirical distribution typically approximates but does not exactly match the true distribution. To address this discrepancy, we assume that the true distribution $\mathbb{Q}$ resides within a Wasserstein ball (Fournier and Guillin, 2015) centered on the empirical distribution $\hat{\mathbb{Q}}_N$, with a radius $\theta \in \mathbb{R}_+$. The resulting ambiguity set of distributions, $\mathcal{F}(\theta)$, is then defined as:

$$\mathcal{F}(\theta) = \{\mathbb{Q} \in \mathcal{M}(\Xi) \mid \tilde{\mathbf{p}} \sim \mathbb{Q}, \hat{\mathbf{p}} \sim \hat{\mathbb{Q}}_N, d_W(\mathbb{Q}, \hat{\mathbb{Q}}_N) \leq \theta\}, \tag{22}$$

where Ξ is the support set, and $d_W(\mathbb{Q}, \hat{\mathbb{Q}}_N)$ denotes the Wasserstein distance between the true distribution $\mathbb{Q}$ and the empirical distribution $\hat{\mathbb{Q}}_N$ (Mohajerin Esfahani and Kuhn, 2018). Under some conditions, the choice of θ as a decreasing function in N affects the confidence that $\mathbb{Q}$ lies within the ambiguity set $\mathcal{F}(\theta)$. As $N \to \infty$, $\theta \to 0$ and $\hat{\mathbb{Q}}_N$ converges to $\mathbb{Q}$. We refer readers to Hanasusanto and Kuhn (2018) for more details. The Wasserstein distance ambiguity set not only accounts for potential outcomes of bunker prices not observed in historical data but also allows for a tractable reformulation of the robust liner service optimization problem. Due to its advantageous properties, the Wasserstein-distance-based metric has become a leading approach for modeling uncertainty in recent years (Hanasusanto and Kuhn, 2018; Mohajerin Esfahani and Kuhn, 2018; Gao and Kleywegt, 2023). The Wasserstein distance is defined as:

$$d_W(\mathbb{Q}, \hat{\mathbb{Q}}_N) = inf\ \mathbb{E}_\Pi[\|\tilde{\mathbf{p}} - \hat{\mathbf{p}}\|] \tag{23}$$

$$s.t.\ \tilde{\mathbf{p}} \sim \mathbb{Q}, \hat{\mathbf{p}} \sim \hat{\mathbb{Q}}_N, (\tilde{\mathbf{p}}, \hat{\mathbf{p}}) \sim \Pi, \tag{24}$$

$$\Pi[(\tilde{\mathbf{p}}, \hat{\mathbf{p}}) \in \Xi \times \Xi] = 1, \tag{25}$$

where Π denotes the joint distribution of $\tilde{\mathbf{p}} \sim \mathbb{Q}$ and $\hat{\mathbf{p}} \sim \hat{\mathbb{Q}}_N$, and $\|.\|$ is the 2-norm distance. With the ambiguity set (22), we can formulate a Wasserstein robust optimization model of the CCP model:

$$[\text{DRCC}]\min \Theta + \sum_{i\in\mathcal{P}}\gamma_i\psi_i + \sum_{(i,j)\in\mathcal{L}}\sum_{s\in\mathcal{S}_{ij}}\sum_{v\in\mathcal{V}_s}\sum_{f\in\mathcal{F}}\eta\phi_f(\Delta_{vf}+\delta_f)t_{sv}^{ij}x_{svf}^{ij} + \sum_{i\in\mathcal{P}}\eta\phi_{LNG}\delta_{LNG}\tau_i \tag{26}$$

$$s.t. \; \inf_{\mathbb{Q} \in \mathcal{M}(\Xi) : d_W(\mathbb{Q}, \hat{\mathbb{Q}}_N) \leq \theta} \mathbb{P}\left[\Theta \geq \sum_{i \in \mathcal{P}} \sum_{f \in \mathcal{F}} \tilde{p}_f^i b_f^i \right] \geq 1 - \varepsilon, \tag{27}$$

$$(2) - (18), \text{and } \Theta \geq 0. \tag{28}$$

The objective function (26) aims to minimize the expected bunker costs, delay costs, and emission costs. Constraint (27) specifies that, given a known discrete empirical distribution of fuel prices $\hat{\mathbb{Q}}_N$ and a probability distribution of fuel prices satisfying the Wasserstein distance, the probability that the actual bunker cost under the worst-case distribution is less than the expected bunker cost Θ is at least $1 - \varepsilon$. Here, ε represents the confidence level of the chance constraint.

3.4. Tractable re-formulation of DRCC model

It should be noted that the DRCC model cannot be solved directly. This section presents an equivalent mixed-integer second-order conic programming (MISOCP) reformulation for the DRCC model. We begin with a theorem and a lemma.

Theorem 1. *The chance constraint (27) over the Wasserstein ambiguity set (22) is equivalent to the following deterministic inequalities:*

$$\varepsilon N \chi - \sum_{n=1}^{N} \varpi_n \geq \theta N, \tag{29}$$

$$\textbf{dist}(\hat{\textbf{p}}_n, \overline{S}(\textbf{b})) \geq \chi - \varpi_n, \forall n \in \{1, 2, \dots, N\}, \tag{30}$$

$$\varpi_n \geq 0, \chi \text{ is free}, \tag{31}$$

where $\overline{S}(\textbf{b}) = \{\tilde{\textbf{p}} \in \Xi | \Theta < \sum_{i \in \mathcal{P}} \sum_{f \in \mathcal{F}} \tilde{p}_f^i b_f^i\}$ represents the unsafe data set that obeys the inequality $\Theta \geq \sum_{i \in \mathcal{P}} \sum_{f \in \mathcal{F}} \tilde{p}_f^i b_f^i$, and $\textbf{dist}(\hat{\textbf{p}}_n, \overline{S}(\textbf{b}))$ denotes the distance of *n-th* sample data point $\hat{\textbf{p}}_n$ from the empirical distribution $\hat{\mathbb{Q}}_N$ to the unsafe set $\overline{S}(\textbf{b})$. The proof of this theorem will be provided after introducing Lemma 1.

Lemma 1. *Let $\{r_1, r_2, \dots, r_N\}$ be a set of real numbers sorted in ascending order by index n. For any $\varepsilon \in (0, 1)$, the sum of the εN smallest elements in this set is equal to the optimal value of the following linear programming model:*

$$\max_{\varpi, \chi} \varepsilon N \chi - \sum_{n=1}^{N} \varpi_n \tag{32}$$

$$s.t. \; r_n \geq \chi - \varpi_n, \forall n \in \{1, 2, \dots, N\}, \tag{33}$$

$$\varpi_n \geq 0, \chi \text{ is free}. \tag{34}$$

Proof of Lemma 1. The sum of εN smallest elements of the set $\{r_1, r_2, \dots, r_N\}$ is equivalent to the optimal value of the linear programming model, according to the strong duality of linear programming:

$$\min_x \sum_{i=1}^{N} r_i x_i \tag{35}$$

$$s.t. \; \sum_{i=1}^{N} x_i = \varepsilon N, \tag{36}$$

$$x_i \in [0, 1], \forall i \in \{1, 2, \dots, N\}. \tag{37}$$

This completes the proof of Lemma 1. □

Proof of Theorem 1. Based on Lemma 1, we can reformulate the chance constraint (27) as inequality $\frac{1}{N} \sum_{n=1}^{\varepsilon N} \textbf{dist}(\hat{\textbf{p}}_{\pi_n(\textbf{b})}, \overline{S}(\textbf{b})) \geq \theta$ using Theorem 2 from Chen et al. (2024), with $\textbf{dist}(\hat{\textbf{p}}_{\pi_1(\textbf{b})}, \overline{S}(\textbf{b})) \leq \textbf{dist}(\hat{\textbf{p}}_{\pi_2(\textbf{b})}, \overline{S}(\textbf{b})) \leq \dots \leq \textbf{dist}(\hat{\textbf{p}}_{\pi_N(\textbf{b})}, \overline{S}(\textbf{b}))$. The left-hand side of this inequality means that a fixed bunkering decision $\textbf{b}$ satisfies the ambiguous chance constraint (27) over the Wasserstein ambiguity set (22) if and only if the partial sum of the εN smallest transportation distances to the unsafe set multiplied by the mass $\frac{1}{N}$ of a training sample exceeds θ (Chen et al., 2024). Therefore, we can use the linear programming model in Lemma 1 to represent the left-hand side of (27) and ultimately obtain the inequalities (29) and (30). This completes the proof of Theorem 1. □

Proposition 1. *In this problem, constraints (29), (30), and (31) are equivalent to the following constraints:*

$$\varepsilon N \chi - \sum_{n=1}^{N} \varpi_n \geq \theta N \|\boldsymbol{b}\|_*, \tag{38}$$
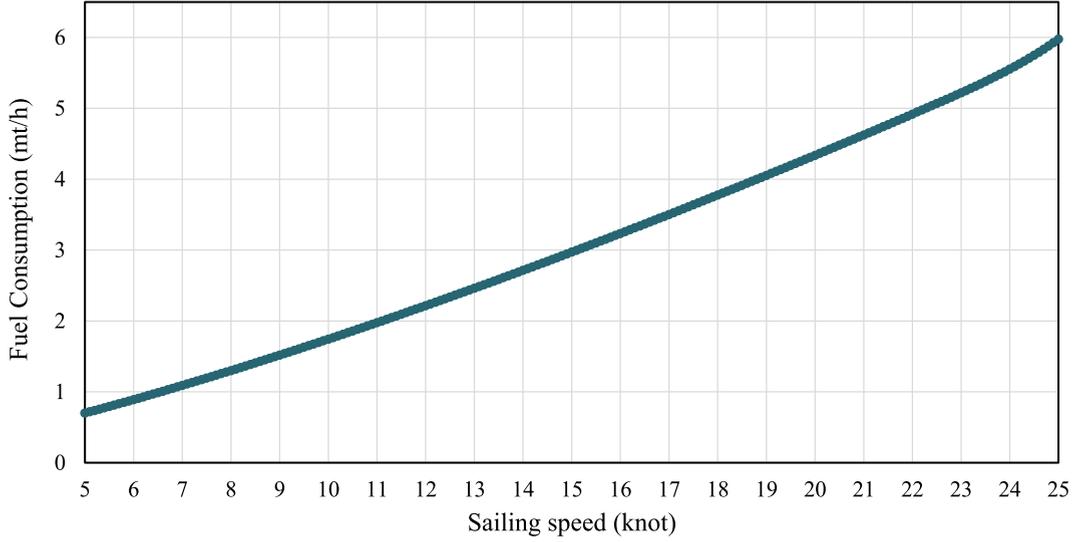
Fig. 3. Hourly fuel consumption of the ship's main engine at different speeds using HFO fuel.

$$\Theta - \sum_{i \in \mathcal{P}} \sum_{f \in \mathcal{F}} \widetilde{p}^i_{f,n} b^i_f + M \ell_n \geq \chi - \varpi_n, \forall n \in \{1, 2, \ldots, N\}, \tag{39}$$

$$M(1 - \ell_n) \geq \chi - \varpi_n, \forall n \in \{1, 2, \ldots, N\}, \tag{40}$$

$$\varpi_n \geq 0, \ell_n \in \{0, 1\}, \forall n \in \{1, 2, \ldots, N\}, \tag{41}$$

$$\Theta \geq 0, \chi \; is \; free, \tag{42}$$

where $\|.\|_*$ is the dual norm of $\|.\|$, and M is a relatively large constant (Chen et al., 2024). See Appendix B for the proof of Proposition 1.

Based on these preparations, we can rewrite the DRCC model as the following mixed-integer second-order conic programming (MISOCP) model:

$$[\text{MISOCP}] \min \Theta + \sum_{i \in \mathcal{P}} \gamma_i \psi_i + \sum_{(i,j) \in \mathcal{L}} \sum_{s \in S_{ij}} \sum_{v \in \mathcal{V}_s} \sum_{f \in \mathcal{F}} \eta \phi_f (\Delta_{vf} + \delta_f) t^{ij}_{sv} x^{ij}_{svf} + \sum_{i \in \mathcal{P}} \eta \phi_{LNG} \delta_{LNG} \tau_i \tag{43}$$

$$s.t. \; (2) - (18) \; \text{and} \; (38) - (42). \tag{44}$$

4. Numerical experiments

The MISOCP model can be directly solved using solvers such as CPLEX or GUROBI. This section presents numerical experiments based on the MISOCP model to (i) evaluate its computation performance, (ii) demonstrate the potential benefits of considering bunker price uncertainty, and (iii) perform sensitivity analyses on key parameters, such as the Wasserstein distance and the price ratio of different fuels. The models are implemented in C++ and solved using CPLEX 12.10. All computational experiments are conducted on a PC equipped with a 64-bit 2.4 GHz processor and 16 GB of RAM.

4.1. Test instances

We consider a 13,500 TEU dual-fuel container ship equipped with fuel tanks for HFO, MGO, and LNG, with capacities of 3000 mt, 4000 mt, and 3000 mt, respectively. The safety inventory levels for these fuels are 200 mt, 200 mt, and 300 mt, respectively. The ship's design speed is 25 knots. The average fuel consumption of HFO at various speeds for the main engine is shown in Fig. 3, while the average fuel consumption of MGO for the auxiliary engine is 0.5 mt per hour. Due to differences in calorific values among these fuels, consumption rates of HFO, MGO, and LNG vary at the same power. As indicated in Table 4, the calorific values of MGO and LNG are 1.07 and 1.25 times that of HFO, respectively. Consequently, the fuel consumption of MGO and LNG can be set to 0.93 and

Table 4
Parameters of fuels.

Fuel	Fuel type	CO_2 emission(g CO_2/ g fuel)	Calorific values(MJ/t)
HFO	Heavy fuel	3.114	40,000
MGO	Light fuel	3.206	42,700
LNG	Light fuel	2.750	50,000

Fig. 4. Locations of ports on six shipping lines.

0.80 times that of HFO at the same sailing speed, respectively. While passing through the Suez Canal and Panama Canal, the ship's speed must be no less than 6 knots.

The ship can be deployed on shipping lines WAX3, WSA4, CAX1, ESA, AEU7, and AEM1 of COSCO Shipping, with the number of ports of call for each line shown in Fig. 4 and the detailed information of each line presented in Appendix C. The number of sub-legs of these lines is presented in Table 5. The penalty cost for delays at each port is set at 20,000 USD per hour. The bunkering setup time is 0.5 hours. The emission cost is 50 USD per ton. Sailing speeds are discretized into intervals of 0.1 knots. Data on fuel prices at these ports are collected from the Clarkson database. We create 200 sets of in-sample data and 200 sets of out-of-sample test data. The parameters θ and ε are set to 0.1 and 0.05, respectively.

4.2. Computational performance of the models

To comprehensively evaluate both the computational performance of the proposed models and the economic/environmental benefits of the fuel-switching capability, we define six distinct cases with different fuel combinations for each shipping line, as detailed in Table 6. The primary rationale for this comparative design is to isolate and quantify the benefit of operational flexibility. Cases 5 & 6, which use single fuels (MGO or LNG only), serve as non-flexible baselines. In contrast, the multi-fuel scenarios (Cases 1 - 4) represent the full fuel-switching flexibility, allowing us to precisely quantify the cost savings and environmental gains achieved by strategically combining different fuels and tank capacities against the single-fuel benchmarks. For consistency in comparison, we assume that the ship uses shore power while berthing at ports. In total, we generate 36 test instances. Additionally, the deterministic model is solved using the average bunker price from sample data. Detailed computation results for both the deterministic and robust models are presented in Table 7.

In terms of computational performance, the deterministic model demonstrates high efficiency, requiring less than 0.3 seconds to solve each instance. In contrast, the MISOCP model exhibits significantly longer computation times, taking up to 2700 seconds to solve some instances. This highlights the increased complexity of the problem under robust optimization frameworks. Regarding objective function values, the MISOCP model shows a 6% increase compared to the deterministic model. This difference arises because the

Table 5

Six shipping lines.

Shipping lines	Port of call	Number of port of call	Number of sub-legs
WAX3	Shanghai–Ningbo–Xiamen–Shekou–Nansha–Singapore–Lome–Tema –Cotonou–Onne–Tema–Kelang–Singapore–Shanghai	14	19
WSA4	Shekou–Hong Kong–Kaohsiung–Ningbo–Shanghai–Busan–Manzanillo (MX) –Lazaro Cardenas–Buenaventura–Callao–Posorja–Lazaro Cardenas– Manzanillo (MX)–Yokohama–Busan–Shekou	16	19
CAX1	Shekou–Hong Kong–Kaohsiung–Ningbo–Shanghai–Qingdao–Busan– Manzanillo (MX)–Balboa–Manzanillo (PA)–Cartagena–Kingston (JM) –Caucedo–Singapore–Shekou	15	22
ESA	Shanghai–Ningbo–Yantian–Hong Kong–Singapore–Rio De Janeiro–Santos –Paranagua–Navegantes–Montevideo–Buenos Aires–Rio Grande–Navegantes –Paranagua–Santos–Singapore–Hong Kong–Shanghai	18	23
AEU7	Shanghai–Xiamen–Nansha–Hong Kong–Yantian–Cai Mep–Singapore–Suez –Piraeus–Hamburg–Rotterdam –Zeebrugge–Valencia–Piraeus–Suez–Aekhl –Kelang–Shanghai	18	27
AEM1	Qingdao–Shanghai–Ningbo–Kaohsiung–Hong Kong–Yantian–Singapore– Suez–Piraeus–La Spezia– Genoa–Fos–Valencia–Piraeus–Suez–Singapore –Qingdao	17	29

Table 6

Six cases with different fuel combinations.

Cases	Combination of fuels	Capacity (mt) of fuel tank	Initial fuel amount (mt)
Case 1	HFO + MGO + LNG	HFO: 3,000, MGO: 4,000, and LNG: 3,000	HFO: 1,000, MGO: 500, and LNG: 1,500
Case 2	HFO + LNG	HFO: 5,000, LNG: 5,000	HFO: 1,500, LNG: 1,500
Case 3	HFO + MGO	HFO: 4,500, MGO:5,500	HFO: 1,500, MGO: 1,500
Case 4	MGO + LNG	MGO: 5,500, LNG: 4,500	MGO: 1,000, LNG:2,000
Case 5	MGO	MGO: 10,000	MGO: 3,000
Case 6	LNG	LNG: 10,000	LNG: 3,000

deterministic model tends to bunker at ports with the lowest bunker prices, while the robust model distributes bunkering across more ports with favorable prices to hedge price uncertainty.

Moreover, the fuel-switching mode can effectively reduce total costs compared to the single-fuel mode. Specifically, it reduces costs by approximately 20.78% and 3.43% compared to using only MGO or LNG, respectively. For high-carbon fuels like MGO, the fuel-switching mode also reduces carbon emissions by approximately 8.74%. However, for low-carbon fuels like LNG, the fuel-switching mode may increase carbon emissions by 21.31%. Consequently, the strategic allocation of alternative-fuel ships across shipping lines is crucial for shipping companies seeking to balance costs and environmental impact.

4.3. Robustness analysis

To evaluate the robustness of the solutions obtained from the MISOCP model, we employ the SAA method to solve the corresponding chance-constrained programming model presented in Appendix A. We then compare the robustness of the solutions obtained from both the MISOCP and SAA models under different training sample sizes. Specifically, we consider training sample sizes of 50, 100, 150, 200, 250, and 300, and generate 100 out-of-sample datasets for each scenario. For each out-of-sample dataset, we assess whether the chance constraint is satisfied under the solutions provided by the MISOCP and SAA models, respectively, and then calculate the percentage of the chance constraint being satisfied.

The experimental results, summarized in Fig. 5, demonstrate the superior robustness of the MISOCP model. Specifically, when the training sample size exceeds 150, the average probability of satisfying the chance constraint for out-of-sample datasets reaches 92%. In comparison, the solutions generated by the SAA method demonstrate weaker robustness, with the probability of satisfying the chance constraint remaining at only 52%, even when the training sample size increases to 300.

To further investigate the performance divergence between the robust and deterministic (non-robust) solutions regarding fuel bunkering costs under price volatility, we conduct a series of comparative simulations based on the six scenarios outlined in Section 4.1, utilizing randomly generated combinations of fuel prices. The computational results are illustrated in Fig. 6. Across all price scenarios, the robust solution demonstrated superior average economic performance. Specifically, the average bunkering cost for the robust solution is $2,860,511, whereas that of the deterministic solution is $2,881,595. This indicates that the robust solution achieves an average cost saving of 0.73% over the deterministic one. Additionally, we assessed the Value at Risk (VaR) of fuel bunkering costs under price volatility. At the 95% confidence level, the VaR for the robust solution was $3,018,930, while the VaR for the deterministic solution reached $3,288,440. This demonstrates that the robust model significantly reduces the potential cost ceiling in extreme scenarios by 8.2%, underscoring its effectiveness in hedging against fuel price volatility.

Table 7
Computational results of deterministic and distributionally robust chance-constraint models.

Instances		Deterministic Model			MISOCP Model		
		Time (seconds)	Obj (10^6 \$)	Emis (10^4 mt)	Time (seconds)	Obj (10^6 \$)	Emis (10^4 mt)
WAX3 line	Case 1	0.23	3.51	1.58	881.16	3.66	1.63
	Case 2	0.11	3.47	1.63	1055.97	3.64	1.67
	Case 3	0.09	3.49	1.68	927.89	3.66	1.68
	Case 4	0.13	3.67	1.19	15.237	3.93	1.19
	Case 5	0.06	4.52	1.62	7.11	4.83	1.62
	Case 6	0.08	3.64	1.19	10.13	3.92	1.19
WSA4 line	Case 1	0.26	4.02	1.64	413.86	4.18	1.71
	Case 2	0.12	4.00	1.82	172.19	4.18	1.72
	Case 3	0.13	4.05	1.84	1339.42	4.24	1.84
	Case 4	0.14	4.06	1.31	144.21	4.37	1.31
	Case 5	0.07	4.98	1.78	63.36	5.34	1.78
	Case 6	0.06	4.05	1.31	27.74	4.37	1.31
CAX1 line	Case 1	0.15	3.50	1.57	803.81	3.65	1.64
	Case 2	0.08	3.48	1.63	1404.22	3.64	1.65
	Case 3	0.09	3.49	1.69	2607.55	3.65	1.69
	Case 4	0.08	3.71	1.20	47.63	3.98	1.19
	Case 5	0.05	4.55	1.63	15.68	4.87	1.63
	Case 6	0.05	3.66	1.19	48.59	3.95	1.19
ESA line	Case 1	0.17	3.44	1.48	142.79	3.60	1.41
	Case 2	0.08	3.44	1.60	341.54	3.60	1.41
	Case 3	0.12	3.45	1.60	1539.59	3.67	1.60
	Case 4	0.1	3.47	1.13	33.88	3.71	1.13
	Case 5	0.05	4.30	1.54	15.89	4.59	1.54
	Case 6	0.06	3.46	1.13	6.97	3.71	1.13
AEU7 line	Case 1	0.23	3.74	1.76	276.92	3.98	1.76
	Case 2	0.11	3.74	1.76	78.65	3.98	1.76
	Case 3	0.14	3.84	1.82	107.45	4.09	1.82
	Case 4	0.16	3.90	1.29	25.22	3.38	1.29
	Case 5	0.06	4.77	1.76	16.21	5.08	1.76
	Case 6	0.07	3.90	1.29	89.56	4.21	1.29
AEM1 line	Case 1	0.23	3.11	1.38	2202.74	3.25	1.25
	Case 2	0.12	3.11	1.38	375.92	3.25	1.25
	Case 3	0.13	3.22	1.44	366.59	3.39	1.44
	Case 4	0.16	3.15	1.02	17.99	3.38	1.02
	Case 5	0.07	3.88	1.39	18.55	4.15	1.39
	Case 6	0.07	3.14	1.02	109.94	3.38	1.02
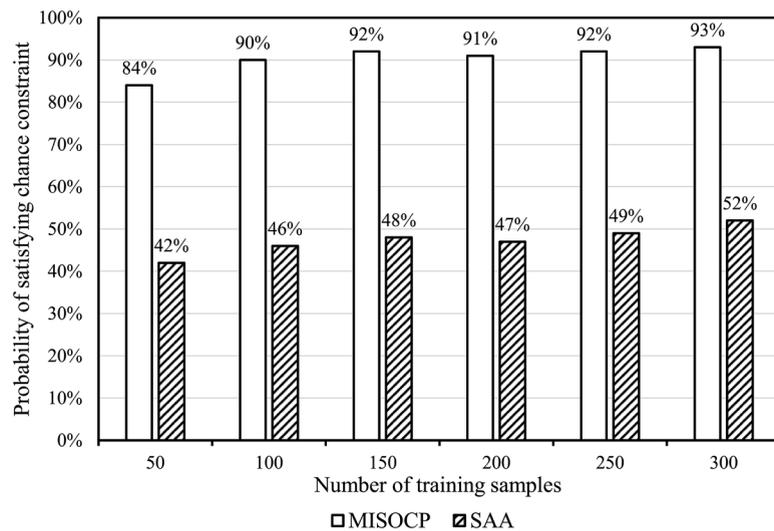
Fig. 5. Comparison of solution robustness between the MISOCP model and the SAA method.
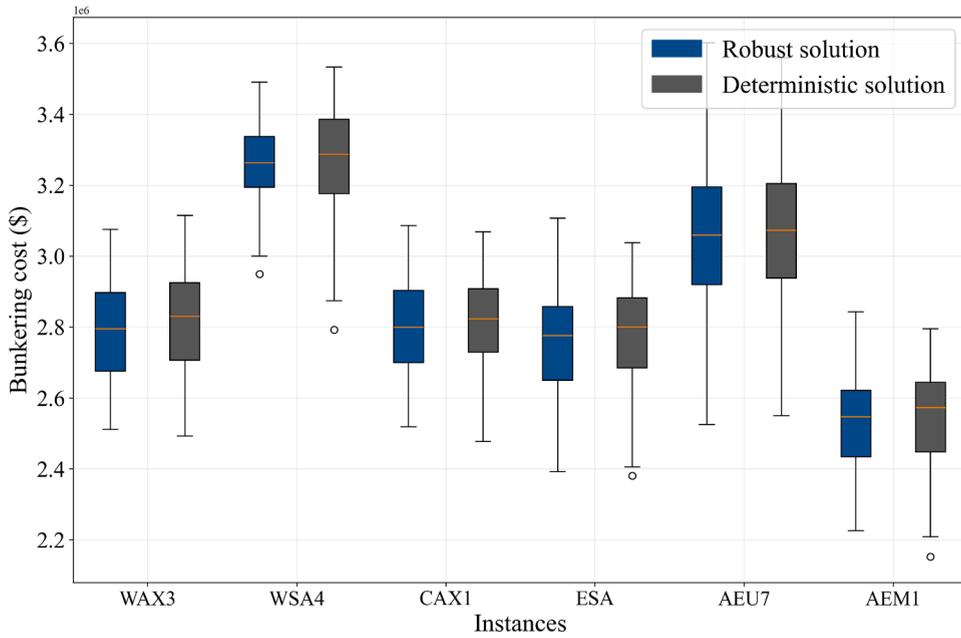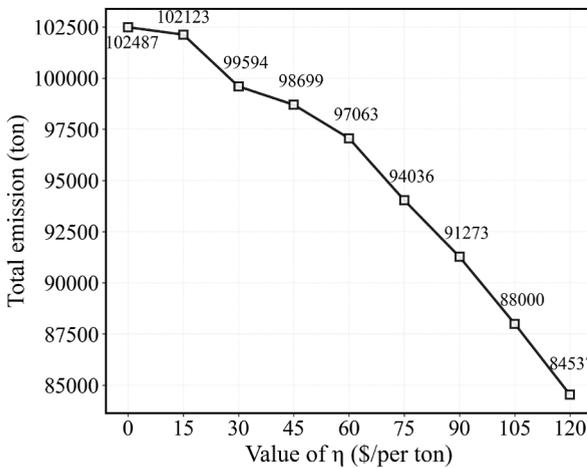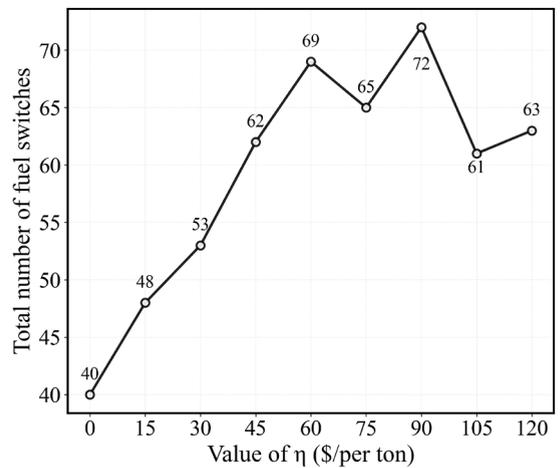
Fig. 6. Bunkering costs for robust and non-robust solutions at different fuel prices.

(a) Total emissions with different η

(b) Total number of fuel switches with different η

Fig. 7. Total emissions and number of fuel switches with different emission penalty coefficients.

Furthermore, it is clearly observable in the figure that the bunkering costs associated with the deterministic solution exhibit greater volatility. This comparison confirms that the proposed robust approach can effectively hedge against the risks posed by fuel price fluctuations, demonstrating cost stability across diverse market conditions.

4.4. Sensitivity analysis on emission penalty coefficient

To analyze the impact of different carbon emission penalty coefficients (η) on liner shipping operations and costs, we use a set of penalty coefficients (0, 15, 30, 45, 60, 75, 90, 105, 120 \$/ton) and conduct numerical experiments based on the six aforementioned shipping lines. The results are presented in Fig. 7 and Fig. 8, where Fig. 7 illustrates the total emissions and total number of fuel switches under different penalty coefficients, and Fig. 8 shows the variation of emission cost, operating cost, and total cost with the penalty coefficient.

As shown in Fig. 7(a), the carbon emissions significantly decrease as the penalty coefficient increases, confirming the effectiveness of economic penalties as a powerful mitigation tool. Specifically, when the coefficient increases from 0 \$/ton to 120 \$/ton, the total emission is reduced from 102,487 tons to 84,537 tons, a notable decrease of 17.51%. However, the impact of emission reduction on the
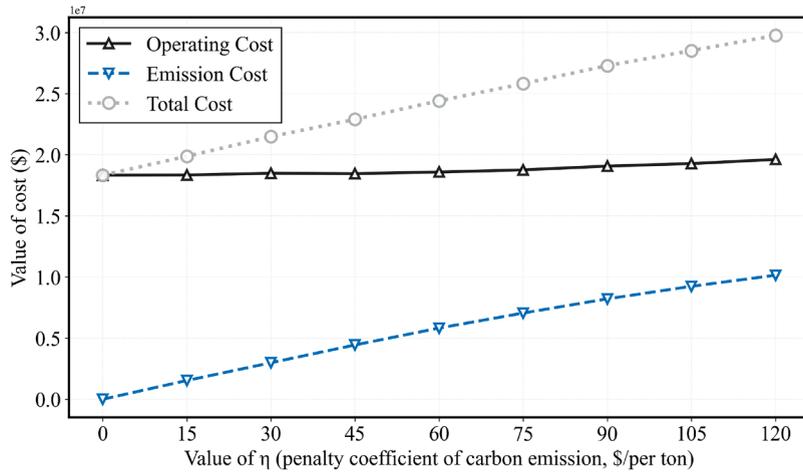
Fig. 8. Cost variation with different emission penalty coefficients.

(a) Fuel usage ratio comparison: with vs without ECA

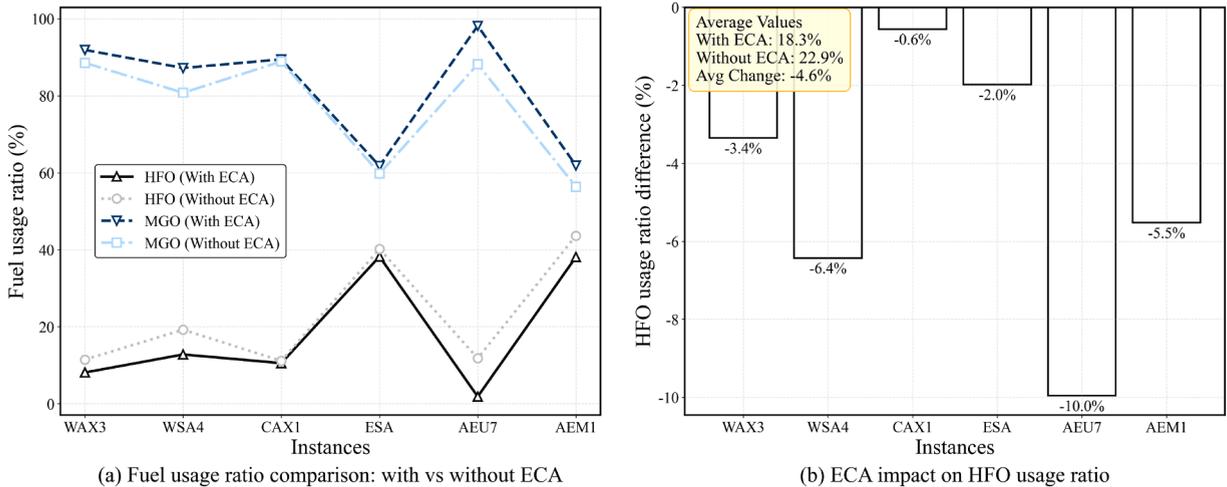(b) ECA impact on HFO usage ratio

Fig. 9. ECA policy impact analysis on fuel usage trends.

operational strategy is a complex, nonlinear relationship. Fig. 7(b) shows that the number of fuel switches does not vary monotonically with the penalty coefficient but reaches a peak at a coefficient of 90 $/ton before subsequently declining. This suggests the existence of a strategic "tipping point": when the carbon price (penalty) is sufficiently high, the vessel's optimal operational strategy shifts from frequent fuel switching to continuous use of clean fuel over longer segments, thereby reducing the switching frequency.

Furthermore, Fig. 8 reveals that as the carbon price increases, the emission cost exhibits a strong, nearly linear upward trend, growing from 0 (at zero carbon price) to approximately 1.01×10^7 (at a carbon price of 120 $/ton). Concurrently, the increased carbon price compels vessels to adopt measures such as utilizing more clean fuel, which is typically more expensive than traditional fuels, and consequently leads to an increase in operating costs. However, the magnitude of the operating cost increase is relatively gradual, rising from approximately 1.83×10^7 to 1.96×10^7, an increase of about 6%. This implies that the operating cost increment brought about by the mitigation measures themselves is far less than the increase in direct emission costs (carbon tax) required to be paid. Consequently, the total cost, as the sum of the former two, also shows a strong, linear growth trend (from approximately 1.83×10^7 to 2.98×10^7). The results above demonstrate that the "Total Cost" is highly sensitive to the "Carbon Price," and a systemic cost increase is inevitable. Therefore, while increasing the carbon price effectively incentivizes emission reduction, it also significantly increases the overall financial burden on shipping companies, primarily driven by mandatory carbon tax payments.

4.5. Impacts of ECAs

To analyze the impact of the ECA policy on fuel usage, numerical experiments are conducted for the aforementioned shipping lines under two distinct scenarios: with and without the ECA regulation. The resulting comparison of fuel usage is presented in
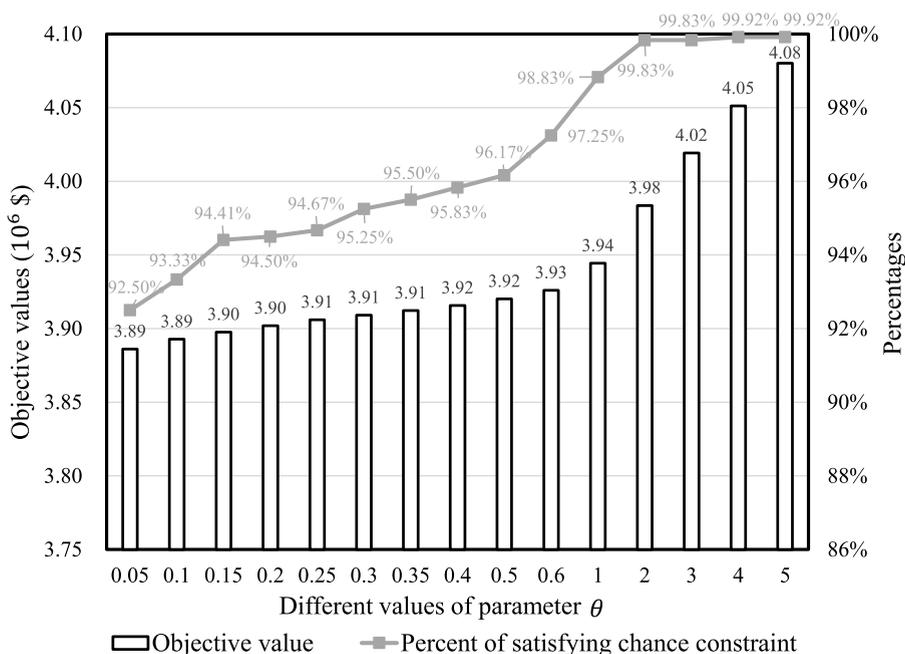
Fig. 10. Sensitivity analysis on parameter θ.

Fig. 9. Specifically, Fig. 9(a) illustrates the ratio of HFO and MGO for each shipping line. Fig. 9(b) highlights the reduction in HFO consumption achieved when the ECA policy is implemented.

The figure indicates that the HFO usage rate under the ECA-included scenario is consistently lower than that without ECA. The average HFO usage rate decreased from 22.9% to 18.3%, a reduction of 4.6%. Meanwhile, the usage rate of MGO is consistently higher when ECA policies are considered. The extent of HFO reduction induced by the ECA policy varies considerably across shipping lines. On the AEU7 shipping line, which passes through multiple ECAs, the HFO usage rate decreased by as much as 10%. In contrast, on the CAX1 shipping line, which traverses fewer ECA zones, the impact was minimal (0.6%). This indicates that the effect of the ECA policy on operational costs and strategies is not uniform but highly dependent on specific shipping line characteristics, such as the proportion of the route within ECAs.

Furthermore, the implementation of the ECA policy leads to adjustments in operational strategies, manifested as an increase in fuel switching frequency. For instance, in the AEU shipping line, considering ECA resulted in 7 additional fuel switches. However, the impact of ECA consideration on both carbon emissions and total cost is negligible: carbon emissions decreased by only 0.73%, while total cost increased by merely 0.06%.

4.6. Sensitivity analysis on wasserstein radius

As the Wasserstein radius, θ, is a key parameter in the distributionally robust optimization model, we analyze its impact by selecting different values of θ and using 200 in-sample training datasets and 200 out-of-sample datasets. The analysis focuses on the average objective value and probability of satisfying the chance constraint for the six shipping lines mentioned earlier. The results are presented in Fig. 10.

Both the objective value and the probability increase as θ rises. Specifically, when θ increases from 0.05 to 5, the probability of satisfying the chance constraint increases from 92.5% to 99.9%. Simultaneously, the objective value rises from 3.8861 to 4.0801 million, representing a 5% increase. This trend occurs because a larger θ allows the model to account for a broader range of uncertainty distributions, thereby increasing the robustness of the solution and, consequently, the objective value.

To further investigate how this robustness (and its associated cost increase) manifests in specific operational metrics, and to contrast it with the deterministic solution, we analyze the impact of θ (from 0 to 0.90) on total emissions and fuel switches. Here, $\theta = 0$ represents the deterministic solution (ignoring uncertainty), while $\theta > 0$ represents the robust solution. The experimental results are presented in Fig. 11.

As shown in Fig. 11, the deterministic solution ($\theta = 0$) achieves the minimum total emission (78,701 tons) and the lowest number of fuel switches (37 times). However, as soon as minimal uncertainty is introduced ($\theta = 0.05$), the total emission immediately jumps by 24.01% to 97,595 tons, and the number of fuel switches surges to 143. For $\theta > 0$, both metrics remain relatively stable at these higher levels, indicating the model shifts to a more robust operational strategy.
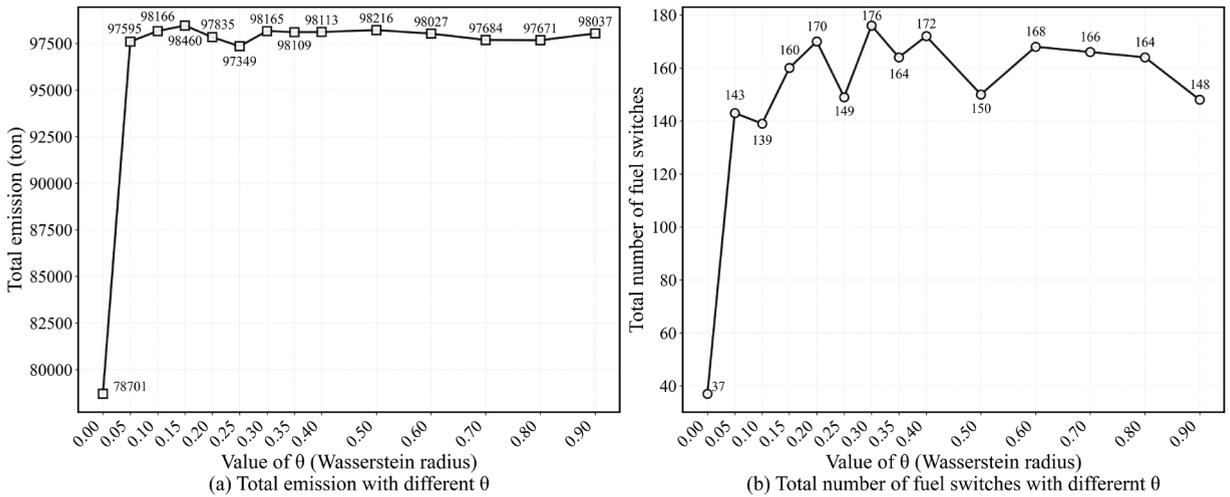
Fig. 11. Total emissions and number of fuel switches with different Wasserstein radius.
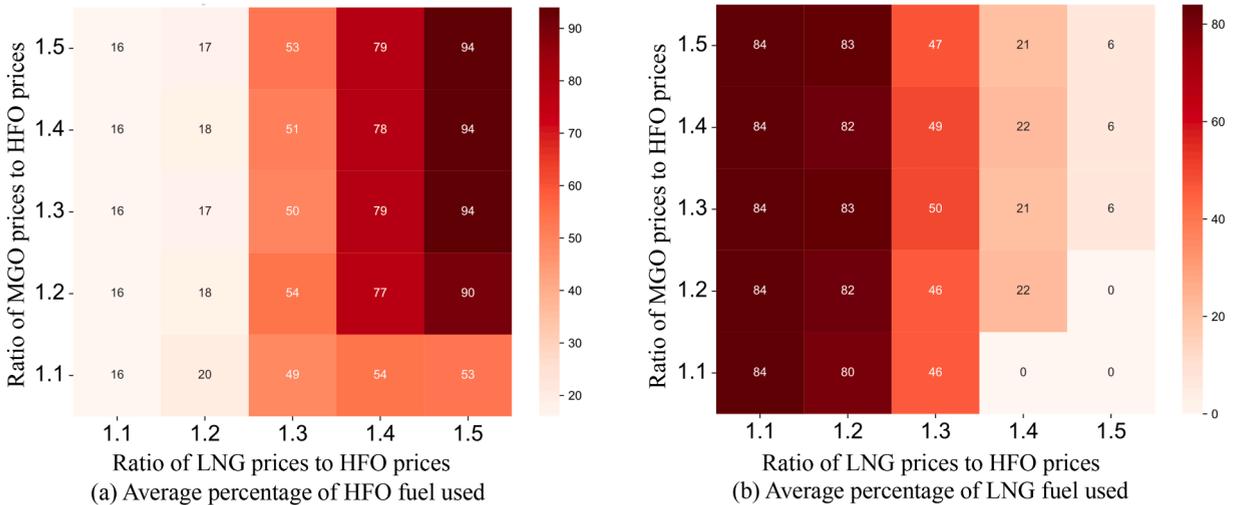

Fig. 12. Fuel usage percentages at different fuel price ratios.

4.7. Sensitivity analysis on fuel price differences

To evaluate the impact of varying fuel price ratios on fuel usage strategies, we generate five price scenarios for both LNG and MGO based on their historical data. The average prices for LNG and MGO in these scenarios are set at 1.1, 1.2, 1.3, 1.4, and 1.5 times the average price of HFO, respectively. This is because the bunker price of HFO is usually the lowest of these fuels. The proportion of each fuel used under different price ratios is then analyzed. We conduct experiments based on data from the six shipping lines described in Section 4.1, with the average usage proportions of LNG and HFO across different fuel price ratios illustrated in Fig. 12 (a) and (b).

The results demonstrate that fuel price ratios significantly influence fuel usage strategies. When the prices of LNG and MGO are only slightly higher than HFO, such as the prices within 1.2 times of HFO, the average usage proportions of LNG and MGO are 83% and 11%, respectively. In such cases, despite LNG's average bunker cost being marginally higher than HFO's, LNG is effective in reducing carbon emissions, leading to lower overall operating costs.

Notably, the average utilization rates for HFO, LNG, and MGO across all scenarios are 49%, 47%, and 4%, respectively. This low utilization of MGO is attributed to its high CO_2 emissions, which result in elevated operating costs under carbon tax regimes and other emissions reduction policies. Consequently, shipping companies should prioritize deploying dual-fuel ships equipped with LNG and HFO under emission reduction policies such as carbon taxes. This might help minimize overall operating costs while adhering to environmental regulations.

4.8. Managerial insights

The extensive numerical experiments yield several insights for shipping companies considering the adoption of dual-fuel ships in liner shipping services.

First, the fuel-switching strategy is a practical approach to balancing cost efficiency and emission reduction. Specifically, it reduces total costs by up to 20.78% compared to single-fuel mode, such as using only MGO. While it might increase emissions by 21.31% compared to only using low-carbon fuel like LNG. To maximize the benefits of dual-fuel technology, shipping operators should strategically deploy dual-fuel ships on routes where economic and environmental goals align. For example, shipping lines with high carbon taxes or strict emission regulations should prioritize low-carbon fuel usage to achieve greater overall benefits.

Second, fuel prices heavily affect fuel usage decisions. For instance, when LNG and MGO prices are only slightly higher than HFO, LNG tends to be the preferred option due to its cost and environmental benefits. In contrast, MGO usage remains low across all scenarios due to its high CO_2 emissions. Policymakers and shipping companies should collaborate to reduce the operational costs of greener fuels through targeted incentives. For example, subsidies for LNG and investments in LNG bunkering infrastructure can encourage its adoption and support more sustainable shipping operations.

Third, robust optimization models provide superior reliability in addressing bunker price uncertainties. Decision-makers should prioritize robust optimization for providing liner shipping services, particularly when dealing with highly volatile bunker prices. Robust models ensure more reliable outcomes, reducing the risk of unforeseen cost escalations.

Fourth, shipping companies should adjust the level of conservatism in their models based on the specific characteristics of their routes. For critical routes with higher price volatility, higher conservatism may be beneficial, whereas less critical routes can prioritize cost efficiency. The conservatism in robust models can be controlled using parameters like the Wasserstein radius.

5. Conclusion

This study addresses the novel operational challenges of integrating LNG dual-fuel ships, a pivotal, high-cost, yet essential technology for maritime decarbonization, into liner services. To minimize the operating cost of dual-fuel ships, we introduce the fuel-switching strategy into liner service operations and formulate a novel dual-fuel liner service optimization problem. This problem incorporates sailing speeds, fuel bunkering and switching, and fuel price uncertainties. We first develop a deterministic mixed-integer linear programming model, followed by a chance-constrained programming model. Next, we establish a distributionally robust chance-constrained programming model based on the Wasserstein uncertainty set, which is subsequently reformulated into a tractable mixed-integer second-order conic programming model.

Extensive numerical experiments, using real-world data, validate the computational performance and applicability of the proposed robust model. Notably, the robust model can obtain optimal solutions for real-scale problems within 2700 seconds using the CPLEX solver and demonstrates excellent robustness on identified solutions. Furthermore, the results indicate that fuel switching can reduce operating costs for these liner services by at least 3.43%. Under carbon emission reduction policies, the combined use of LNG and HFO fuels yields the greatest cost savings for LNG dual-fuel ships. The findings provide valuable insights for shipping companies striving to optimally integrate emerging green technologies into their liner services, thereby contributing to the sustainable and cost-effective transformation of global shipping in the era of new energy.

While this study focuses on optimizing dual-fuel liner shipping services and provides valuable insights for shipping operators, it has several limitations. First, the study assumes fixed port times, without accounting for potential fluctuations that may increase delay costs at ports. Extending the robust model to incorporate port time uncertainties could further enhance the reliability and robustness of the solutions. Second, this study focuses on the operational aspects of liner shipping services, while some macro-level decisions are unaddressed. For instance, before LNG or methanol dual-fuel ships are widely adopted in the shipping market, mixed fleets comprising conventional and dual-fuel ships are likely to dominate. Future research should investigate the re-optimization of liner shipping networks and fleet deployment for such mixed fleets. This represents a significantly more complex decision-making problem than the traditional one, necessitating high-quality solution algorithms, such as branch-and-price-and-cut, to solve it effectively. Third, we assume fixed sailing paths between ports. Future research could explore integrating tactical shipping path design into the optimization of liner services to better exploit fuel cost variations and ECA impacts.

CRediT authorship contribution statement

Ping He: Writing – original draft, Methodology, Formal analysis; **Lingxiao Wu:** Writing – review & editing, Data curation, Conceptualization; **Jian Gang Jin:** Writing – review & editing, Conceptualization; **Shaorui Zhou:** Writing – review & editing, Investigation; **Frederik Schulte:** Writing – review & editing, Investigation.

Data availability

Data will be made available on request.

Declaration of competing interest

The authors declare that they have no known competing financial interests or personal relationships that could have appeared to influence the work reported in this paper.

Appendix A. Solving the CCP model via the SAA method

To solve the chance-constrained programming model with uncertain parameter $\tilde{p}_f^i$, which lacks common distributional characteristics, the SAA method is employed. The detailed steps are as follows:

Step 1: Approximation of the chance constraint

We obtain N samples of the uncertain parameter, denoted as $\tilde{p}_{f,1}^i, \tilde{p}_{f,2}^i, \ldots, \tilde{p}_{f,N}^i$, from historical data. Then, the original chance constraint can be replaced by the following sample average approximation:

$$\frac{1}{N} \sum_{n=1}^{N} \mathbb{I}\left[\Theta \geq \sum_{i \in \mathcal{P}} \sum_{f \in \mathcal{F}} \tilde{p}_{f,n}^i b_f^i \right] \geq 1 - \varepsilon, \tag{A.1}$$

where $\mathbb{I}[\cdot]$ is an indicator function that equals 1 if the condition inside is satisfied and 0 otherwise.

Step 2: Linearization

Since the indicator function $\mathbb{I}[\cdot]$ is non-linear and non-differentiable, we introduce a binary auxiliary variable $z_n \in \{0, 1\}$ such that:

$$z_n = \begin{cases} 1, & \text{if } \Theta \geq \sum_{i \in \mathcal{P}} \sum_{f \in \mathcal{F}} \tilde{p}_{f,n}^i b_f^i, \\ 0, & \text{otherwise.} \end{cases} \tag{A.2}$$

So, this condition can be reformulated as:

$$\Theta \geq \sum_{i \in \mathcal{P}} \sum_{f \in \mathcal{F}} \tilde{p}_{f,n}^i b_f^i - M(1 - z_n), \tag{A.3}$$

where M is a sufficiently large constant. Accordingly, the chance constraint becomes:

$$\frac{1}{N} \sum_{n=1}^{N} z_n \geq 1 - \varepsilon. \tag{A.4}$$

Step 3: Reformulation into MILP

Finally, we can get the reformulated model, which is also a Mixed-Integer Linear Programming (MILP) formulation:

$$\min \Theta + \sum_{i \in \mathcal{P}} \gamma_i \psi_i + \sum_{(i,j) \in \mathcal{L}} \sum_{s \in \mathcal{S}_{ij}} \sum_{v \in \mathcal{V}_s} \sum_{f \in \mathcal{F}} \eta \phi_f (\Delta_{vf} + \delta_f) t_{sv}^{ij} x_{svf}^{ij} + \sum_{i \in \mathcal{P}} \eta \phi_{LNG} \delta_{LNG} \tau_i \tag{A.5}$$

$$\text{s.t.} \quad \Theta \geq \sum_{i \in \mathcal{P}} \sum_{f \in \mathcal{F}} \tilde{p}_{f,n}^i b_f^i - M(1 - z_n), \quad \forall n \in \{1, 2, \ldots, N\}, \tag{A.6}$$

$$\frac{1}{N} \sum_{n=1}^{N} z_n \geq 1 - \varepsilon, \tag{A.7}$$

$$(2) - (18), \ \Theta \geq 0, \ z_n \in \{0, 1\}. \tag{A.8}$$

We can directly solve this MILP model via off-the-shelf solvers such as CPLEX or GUROBI to obtain the approximate solution of the original CCP model.

Appendix B. Proof of Proposition 1

In this problem, the **dist**$(\hat{\mathbf{p}}_n, \overline{S}(\mathbf{b}))$ equals $\frac{(\Theta - \sum_{i \in \mathcal{P}} \sum_{f \in \mathcal{F}} \tilde{p}_{f,n}^i b_f^i)^+}{\| \sum_{i \in \mathcal{P}} \sum_{f \in \mathcal{F}} \tilde{p}_{f,n}^i b_f^i \|_*}$ based on the Lemma A.1 presented in Chen et al. (2024). Thus, we can reformulate constraints (30) as:

$$\frac{(\Theta - \sum_{i \in \mathcal{P}} \sum_{f \in \mathcal{F}} \tilde{p}_{f,n}^i b_f^i)^+}{\| \sum_{i \in \mathcal{P}} \sum_{f \in \mathcal{F}} \tilde{p}_{f,n}^i b_f^i \|_*} \geq \chi - \varpi_n, \forall n \in \{1, 2, \ldots, N\}. \tag{B.1}$$

However, constraints (B.1) are not convex due to the existence of maximum operators and fractions of convex functions. We can apply the variable substitutions $\chi \leftarrow \chi / \| \sum_{i \in \mathcal{P}} \sum_{f \in \mathcal{F}} \tilde{p}_{f,n}^i b_f^i \|_*$ and $\varpi_n \leftarrow \varpi_n / \| \sum_{i \in \mathcal{P}} \sum_{f \in \mathcal{F}} \tilde{p}_{f,n}^i b_f^i \|_*$ to rewrite constraints (B.1) as:

$$(\Theta - \sum_{i \in \mathcal{P}} \sum_{f \in \mathcal{F}} \widetilde{p}^i_{f,n} b^i_f)^+ \geq \chi - \varpi_n, \forall n \in \{1, 2, \ldots, N\}. \tag{B.2}$$

Similarly, we need to rewrite constraints (29) as:

$$\varepsilon N \chi - \sum_{n=1}^{N} \varpi_n \geq \theta N \| \sum_{i \in \mathcal{P}} \sum_{f \in \mathcal{F}} \widetilde{p}^i_{f,n} b^i_f \|_*. \tag{B.3}$$

To eliminate the maximum operators, we introduce a binary variable ℓ_n. Thus, we can rewrite constraints (B.2) as the following two sets of constraints:

$$\Theta - \sum_{i \in \mathcal{P}} \sum_{f \in \mathcal{F}} \widetilde{p}^i_{f,n} b^i_f + M \ell_n \geq \chi - \varpi_n, \forall n \in \{1, 2, \ldots, N\}, \tag{B.4}$$

$$M(1 - \ell_n) \geq \chi - \varpi_n, \forall n \in \{1, 2, \ldots, N\}. \tag{B.5}$$

Now, we can rewrite constraints (29) and (30) as constraints (38) to (42). Hence, the proposition is proved. □

Appendix C. Detailed information for the six shipping lines in Fig 4

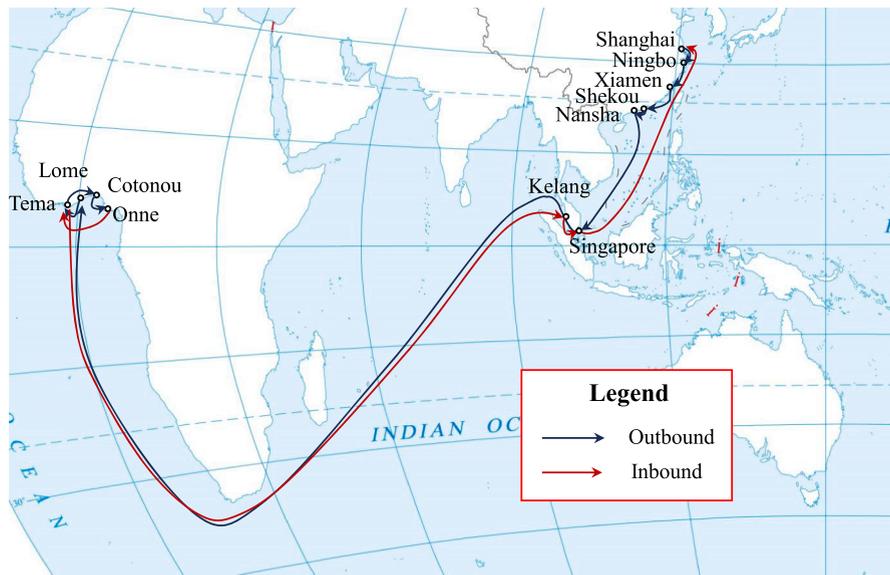**Fig. C.13.** The WAX3 shipping line.

Fig. C.14. The WSA4 shipping line.

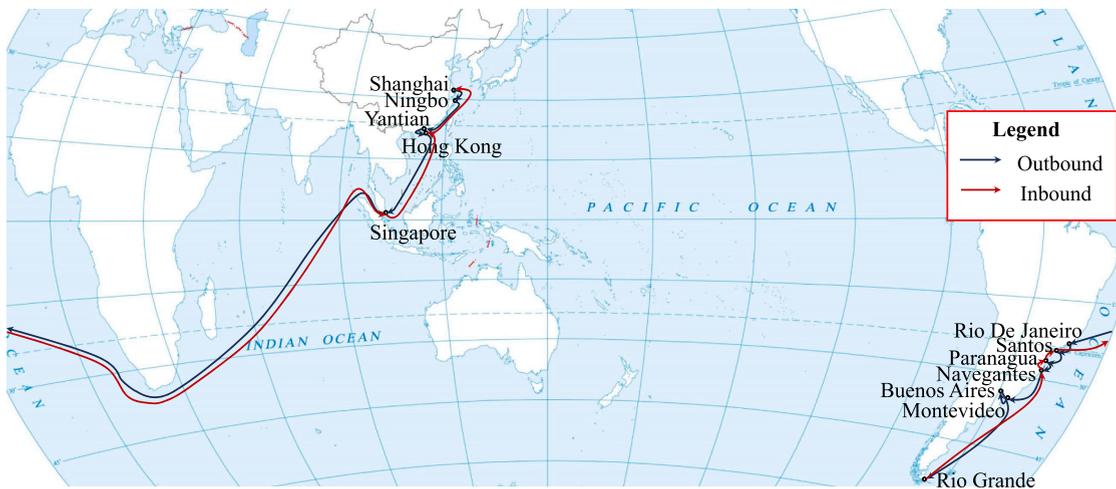**Fig. C.15.** The CAX1 shipping line.
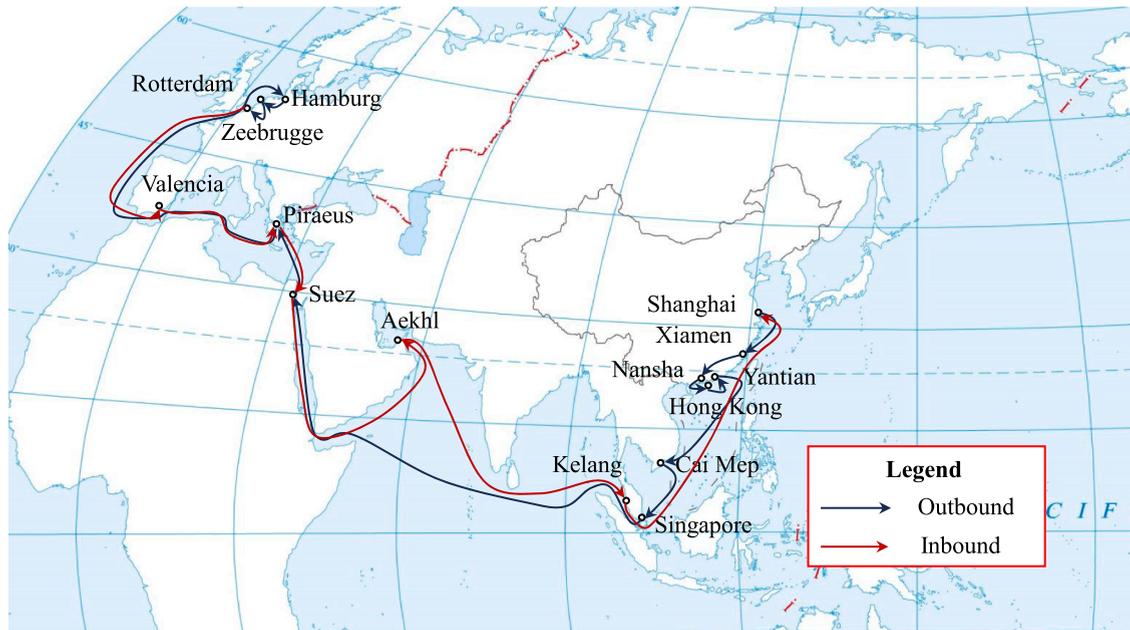

Fig. C.16. The ESA shipping line.
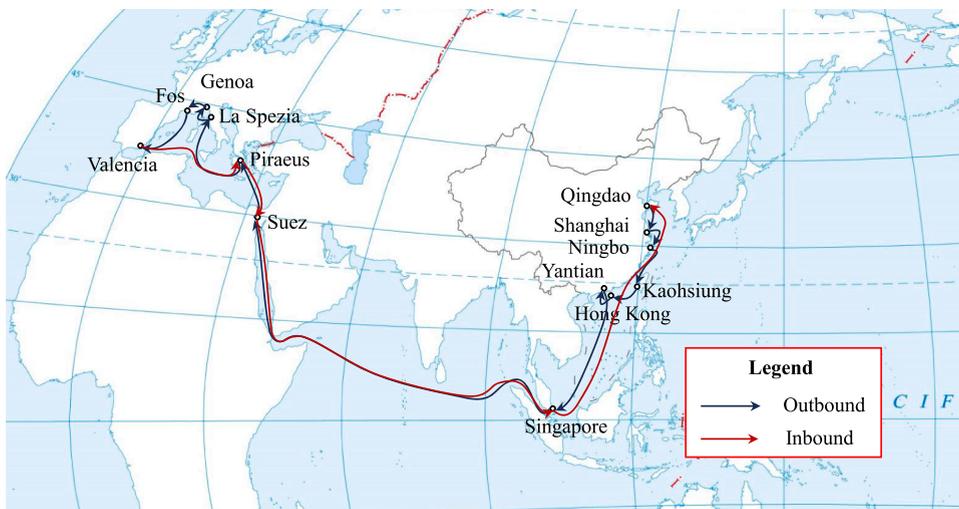
Fig. C.17. The AEU7 shipping line.

Fig. C.18. The AEM1 shipping line.

References

Aydin, N., Lee, H., Mansouri, S.A., 2017. Speed optimization and bunkering in liner shipping in the presence of uncertain service times and time windows at ports. Eur. J. Oper. Res. 259 (1), 143–154.

Balcombe, P., Brierley, J., Lewis, C., Skatvedt, L., Speirs, J., Hawkes, A., Staffell, I., 2019. How to decarbonise international shipping: options for fuels, technologies and policies. Energy Convers. Manage. 182, 72–88.

Chen, Z., Kuhn, D., Wiesemann, W., 2024. Technical note—data-Driven chance constrained programs over wasserstein balls. Oper. Res. 72 (1), 410–424.

Fagerholt, K., Gausel, N.T., Rakke, J.G., Psaraftis, H.N., 2015. Maritime routing and speed optimization with emission control areas. Transp. Res. Part C: Emerg. Technol. 52, 57–73.

Fagerholt, K., Laporte, G., Norstad, I., 2010. Reducing fuel emissions by optimizing speed on shipping routes. J. Oper. Res. Soc. 61 (3), 523–529.

Fagerholt, K., Psaraftis, H.N., 2015. On two speed optimization problems for ships that sail in and out of emission control areas. Transp. Res. Part D: Transp. Environ. 39, 56–64.

Fournier, N., Guillin, A., 2015. On the rate of convergence in wasserstein distance of the empirical measure. Probab. Theory Relat. Fields 162 (3), 707–738.

Gao, R., Kleywegt, A., 2023. Distributionally robust stochastic optimization with wasserstein distance. Math. Oper. Res. 48 (2), 603–655.

Gao, T., Tian, J., Liu, C., Huang, C., Wu, H., Yuan, Z., 2025. A model for speed and fuel refueling strategy of methanol dual-fuel liners with emission control areas. Transp. Policy (Oxf.) 161, 1–16.

Golias, M.M., Saharidis, G.K., Boile, M., Theofanis, S., Ierapetritou, M.G., 2009. The berth allocation problem: optimizing vessel arrival time. Maritime Econ. Logistic. 11, 358–377.

Hanasusanto, G.A., Kuhn, D., 2018. Conic programming reformulations of two-stage distributionally robust linear programs over wasserstein balls. Oper. Res. 66 (3), 849–869.

He, P., Jin, J.G., Pan, W., Chen, J., 2024. Route, speed, and bunkering optimization for LNG-fueled tramp ship with alternative bunkering ports. Ocean Eng. 305, 117957.

Lashgari, M., Akbari, A.A., Nasersarraf, S., 2021. A new model for simultaneously optimizing ship route, sailing speed, and fuel consumption in a shipping problem under different price scenarios. Appl. Ocean Res. 113, 102725.

Li, S., Zhang, P., Sun, Z., 2023. Optimization of fuel supply strategy for LNG dual-fuel ships. J. Phys. Conf. Ser. 2491 (1), 012014.

Li, Y., Jin, J.G., He, P., Lu, C., 2025. Optimizing bunkering and speed for dry bulk carriers considering biofuel storage period limitation. Ocean Coast. Manag. 260, 107482.

Liu, M., Liu, X., Chu, F., Zhu, M., Zheng, F., 2019. Liner ship bunkering and sailing speed planning with uncertain demand. Comput. Appl. Math. 39 (1), 22.

Meng, Q., Wang, S., Lee, C.-Y., 2015. A tailored branch-and-price approach for a joint tramp ship routing and bunkering problem. Transp. Res. Part B: Methodol. 72, 1–19.

Mohajerin Esfahani, P., Kuhn, D., 2018. Data-driven distributionally robust optimization using the wasserstein metric: performance guarantees and tractable reformulations. Math. Program. 171 (1), 115–166.

Norstad, I., Fagerholt, K., Laporte, G., 2011. Tramp ship routing and scheduling with speed optimization. Transp. Res. Part C: Emerg. Technol. 19 (5), 853–865.

Omholt-Jensen, S., Fagerholt, K., Meisel, F., 2025. Fleet repositioning in the tramp ship routing and scheduling problem with bunker optimization: a matheuristic solution approach. Eur. J. Oper. Res. 321 (1), 88–106.

Psaraftis, H.N., Kontovas, C.A., 2014. Ship speed optimization: concepts, models and combined speed-routing scenarios. Transp. Res. Part C: Emerg. Technol. 44, 52–69.

Ronen, D., 2011. The effect of oil price on containership speed and fleet size. J. Oper. Res. Soc. 62 (1), 211–216.

Shangguan, Y., Tian, X., Pang, K.-W., Wang, S., 2025. Optimizing dual-fuel ship operations considering methane slip. Transp. Res. Part B: Methodol. 198, 103247.

Sheng, X., Chew, E.P., Lee, L.H., 2015. (S , s) policy model for liner shipping refueling and sailing speed optimization problem. Transp. Res. Part E: Logist. Transp. Rev. 76, 76–92.

Tan, R., Duru, O., Thepsithar, P., 2020. Assessment of relative fuel cost for dual fuel marine engines along major asian container shipping routes. Transp. Res. Part E: Logist. Transp. Rev. 140, 102004.

UNCTAD, 2019. Review of maritime transport 2019. UN.

Wang, S., Gao, S., Tan, T., Yang, W., 2019. Bunker fuel cost and freight revenue optimization for a single liner shipping service. Comput. Oper. Res. 111, 67–83.

Wang, S., Meng, Q., 2015. Robust bunker management for liner shipping networks. Eur. J. Oper. Res. 243 (3), 789–797.

Wang, S., Zhuge, D., Zhen, L., Lee, C.-Y., et al., 2021. Liner shipping service planning under sulfur emission regulations. Transp. Sci. 55 (2), 491–509. Publisher: INFORMS.

Wang, T., Xia, L., Wang, Y., 2025a. Carbon emissions reduction in maritime supply chain under cap-and-trade and carbon tax policies. Transp. Policy (Oxf.) , 103815.

Wang, Y., Meng, Q., Kuang, H., 2018. Jointly optimizing ship sailing speed and bunker purchase in liner shipping with distribution-free stochastic bunker prices. Transp. Res. Part C: Emerg. Technol. 89, 35–52.

Wang, Y., Zhu, S., Iris, Ç., 2025b. An exact algorithm for fleet co-deployment and slot co-chartering in a sustainable shipping alliance under emissions trading system. Eur. J. Oper. Res. 327(2), 450–468.

Wu, L., Wang, S., Laporte, G., 2021. The robust bulk ship routing problem with batched cargo selection. Transp. Res. Part B: Methodol. 143, 124–159.

Wu, Y., Guo, H., Qi, J., Wang, S., Zhen, L., 2024. Ship refueling optimization for dual-fuel ships considering carbon intensity indicator rating limit and uncertain fuel prices. Multimodal Transp. 3 (3), 100138.

Zhen, L., Hu, Z., Yan, R., Zhuge, D., Wang, S., 2020. Route and speed optimization for liner ships under emission control policies. Transp. Res. Part C: Emerg. Technol. 110, 330–345.

Zhen, L., Wang, S., Zhuge, D., 2017. Dynamic programming for optimal ship refueling decision. Transp. Res. Part E: Logist. Transp. Rev. 100, 63–74.

Zhen, L., Zhuge, D., Zhang, S., Wang, S., Psaraftis, H.N., et al., 2024. Optimizing sulfur emission control areas for shipping. Transp. Sci. 58 (3), 614–638.

Zhou, Y., Wang, C., 2025. Decisions on ship route, refueling, and sailing speed considering ECA regulation and demand uncertainty. J. Oper. Res. Soc. 76 (1), 14–33.

Zhuge, D., Wang, S., Wang, D. Z.W., et al., 2021. A joint liner ship path, speed and deployment problem under emission reduction measures. Transp. Res. Part B: Methodol. 144, 155–173.

Zhuge, D., Wang, S., Zhen, L., 2024. Shipping emission control area optimization considering carbon emission reduction. Oper. Res. 72 (4), 1333–1351.